

RANDOMIZED STRONG RECURSIVE SKELETONIZATION:
SIMULTANEOUS COMPRESSION AND LU FACTORIZATION OF HIERARCHICAL MATRICES
USING MATRIX-VECTOR PRODUCTS

Anna Yesypenko and Per-Gunnar Martinsson
The University of Texas at Austin

Abstract: The hierarchical matrix framework partitions matrices into subblocks that are either small or of low numerical rank, enabling linear storage complexity and efficient matrix-vector multiplication. This work focuses on the \mathcal{H}^2 -matrix format, whose defining feature is the nested basis property which allows basis matrices to be reused across different levels of the hierarchy. While \mathcal{H}^2 -matrices support fast Cholesky and LU factorizations, implementing these methods is challenging—especially for 3D PDE discretizations—due to the complexity of nested recursions and recompressions. Moreover, compressing \mathcal{H}^2 -matrices becomes particularly difficult when only matrix-vector multiplication operations are available.

This paper introduces an algorithm that simultaneously compresses and factorizes a general \mathcal{H}^2 -matrix, using only the action of the matrix and its adjoint on vectors. The number of required matrix-vector products is independent of the matrix size, depending only on the problem geometry and a rank parameter that captures low-rank interactions between well-separated boxes. The resulting LU factorization is invertible and can serve as an approximate direct solver, with its accuracy influenced by the spectral properties of the matrix.

To achieve competitive sample complexity, the method uses dense Gaussian test matrices without explicitly encoding structured sparsity patterns. Samples are drawn only once at the start of the algorithm; as the factorization proceeds, structure is dynamically introduced into the test matrices through efficient linear algebraic operations. Numerical experiments demonstrate the algorithm’s robustness to indefiniteness and ill-conditioning, as well as its efficiency in terms of sample cost for challenging problems arising from both integral and differential equations in 2D and 3D.

1. INTRODUCTION

Dense matrices arising in mathematical physics often exhibit internal structures that enable the efficient solution of problems involving elliptic partial differential equations (PDEs). In many cases, a dense matrix can be partitioned into subblocks where each is either small or admits a compressed representation. Early methods such as the Fast Multipole Method (FMM) [21] leveraged these properties to accelerate matrix-vector operations for a specific class of matrices. Later, the \mathcal{H}^2 -matrix methodology [8, 12, 24] reinterpreted the FMM in algebraic terms by representing off-diagonal subblocks as approximately low rank, thereby extending fast algorithmic techniques to a broader class of matrices. Suppose we have a dense matrix $\mathbf{A} \in \mathbb{R}^{N \times N}$ that is compressible as an \mathcal{H}^2 matrix and that a fast matrix-vector product algorithm is available. In this case, the linear system

$$(1) \quad \mathbf{A} \mathbf{u} = \mathbf{f}$$

can be solved using iterative methods. However, these methods may exhibit unsatisfactory convergence or may be impractical when solving for multiple right-hand sides.

The \mathcal{H}^2 -matrix methodology not only enables fast matrix-vector products but also supports operations such as matrix-matrix multiplication and invertible factorization in linear complexity. However, implementing these algorithms, especially for matrices from three-dimensional PDE discretizations, remains challenging. In this work, we focus on direct inversion techniques for \mathcal{H}^2 matrices under the strong admissibility condition. Key to this format are two distinct features. First, the \mathcal{H}^2 notation refers to a dual-hierarchy structure that achieves linear complexity through

recursive partitioning and the use of nested bases. The representation captures interactions at multiple scales via a tree-based geometric partitioning, with low-rank bases from finer levels successively incorporated into coarser levels. Second, the strong admissibility condition determines which interactions are compressed as low rank: interactions between a box and sufficiently distant boxes are approximated in low rank, while those with neighboring boxes are stored densely. This approach, inspired by the Fast Multipole Method (FMM) [6, 21], is optimal for compressing matrices derived from surfaces or volumes in 3D. The storage cost scales linearly with the number of degrees of freedom N , with a constant that depends on the geometry and compression rank.

Despite the advantages this matrix format offers, the practical use of \mathcal{H}^2 inversion algorithms under the strong admissibility condition has been limited by two core challenges:

- (1) **Compression as \mathcal{H}^2 .** While there exist efficient techniques for obtaining an \mathcal{H}^2 representation of a matrix in certain environments where matrix entries are explicitly available (including adaptive cross approximation [7, 9] and proxy point techniques [47, 48]), the case where \mathbf{A} is only available through its action of vectors remains open. There exist randomized techniques [31] that resolve the problem in principle, but the prefactors involved tend to be very large.
- (2) **Invertible factorization of an \mathcal{H}^2 matrix.** The problem of inverting an \mathcal{H}^2 matrix remains highly challenging, with existing methods relying either on repeated recompressions in recursive structures [8, 10], or on highly storage intensive data structures [40, 42]. (There do exist much faster algorithms for specialized subclasses of matrices [26, 39, 44], but these tend to not be suitable for problems in general geometries in three dimensions.)

This manuscript introduces Randomized Strong Recursive Skeletonization (RSRS), an algorithm that *simultaneously* compresses and inverts \mathcal{H}^2 matrices under the strong admissibility condition. The algorithm produces the “Strong Recursive Skeletonization SRS” factorization introduced in [40] and further improved in [42] (cf. also [3]). RSRS broadens the applicability of \mathcal{H}^2 inversion to a wide range of dense matrices for which fast matrix-vector products for the matrix and its adjoint are available (in contrast [40, 42] which assume that matrix entries of \mathbf{A} are readily available). Specifically, assume that $\mathbf{A} \in \mathbb{R}^{N \times N}$ is an \mathcal{H}^2 matrix with geometric information for its rows and columns, and that a fast method exists to apply both \mathbf{A} and its adjoint \mathbf{A}^* to vectors. RSRS draws two tall thin matrices $\mathbf{\Omega}$ and $\mathbf{\Psi}$ from a standardized normal distribution (so that $\mathbf{\Omega}, \mathbf{\Psi} \sim \mathcal{N}(\mathbf{0}, \mathbf{I})$ are Gaussian matrices), and then generates random sketches [37, Sec. 10],

$$(2) \quad \mathbf{Y}_{N \times s} = \mathbf{A}_{N \times N} \mathbf{\Omega}_{N \times s} \quad \text{and} \quad \mathbf{Z}_{N \times s} = \mathbf{A}^*_{N \times N} \mathbf{\Psi}_{N \times s}.$$

The method then reconstructs an approximate invertible factorization of \mathbf{A} by post-processing

$$\left\{ \mathbf{Y}_{N \times s}, \mathbf{Z}_{N \times s}, \mathbf{\Omega}_{N \times s}, \mathbf{\Psi}_{N \times s} \right\}$$

without directly accessing individual entries of \mathbf{A} . The number of samples s needed depends linearly on the maximal rank of the off-diagonal blocks, but is independent of the matrix dimension N .

RSRS is immediately applicable in a range of important environments. As a solver for boundary integral equations, RSRS can be used to compute an approximate inverse of any integral operator \mathbf{A} for which a fast matrix-vector multiplication algorithm, such as the Fast Fourier Transform (FFT) [17] or the FMM [21, 22], is available. As a solver for PDE discretizations, RSRS can greatly accelerate and simplify algebraic operations of dense operators that arise during the course of a sparse LU factorization. The rank structure in these dense operators can be exploited to achieve competitive complexity and high practical performance in sparse direct solvers [4, 32, 34, 46, 49]. In uncertainty quantification, RSRS may be useful in factorizing the Hessian or dense operators related to the Jacobian, which arise in PDE-constrained optimization problems [1, 2, 27].

1.1. Key Insights and Contributions. The task of recovering hierarchical matrices from matrix–vector products is an active research area, with wider implications to the recovery of structured representations of PDE models from data [13, 14]. A key challenge in black-box randomized algorithms is designing test vectors that allow for approximate matrix recovery with competitive sample complexity, that is, using as few matrix–vector products as possible. Some previous works [31, 33, 38] rely on accessing matrix entries or on designing test matrices with carefully placed zeros to (1) sketch low-rank subblocks and (2) extract small subblocks. However, for LU factorization of \mathcal{H}^2 matrices, such techniques can increase sample complexity and complicate practical implementation. **RSRS** avoids these issues by employing generic dense Gaussian test matrices and leveraging specialized randomized sketching techniques introduced in [28, 29]. Any required structure is imposed via linear transformations applied to the test matrices, rather than by explicitly encoding sparsity patterns or fixed zeros.

The algorithm **RSRS** simultaneously compresses and factorizes the matrix, representing a significant departure from traditional methods that treat these stages separately. Previous work on black-box randomized algorithms for rank-structured matrices [29, 31, 33, 38, 45] has primarily focused on weak admissibility due to its simplicity and the availability of exact inversion algorithms [15, 19, 44]. In contrast, strong admissibility poses additional challenges, such as the need for repeated recompression of off-diagonal blocks during inversion, which has historically limited its application to large 3D problems [3, 8, 10]. Compared to previous algorithms for \mathcal{H}^2 inversion, **RSRS** introduces key innovations by combining the compression and inversion steps, leading to improved computational efficiency and reduced storage requirements, as the updated off-diagonal blocks are stored in compressed form, rather than being stored explicitly.

A core idea motivating our approach is how randomized sketching behaves under multiplicative transformations. Suppose we are given a randomized sample pair $(\mathbf{Y}, \mathbf{\Omega})$ such that $\mathbf{Y} = \mathbf{A}\mathbf{\Omega}$. Now consider an updated matrix $\hat{\mathbf{A}}$ obtained by applying invertible left and right transformations:

$$\hat{\mathbf{A}} = \mathbf{L}\mathbf{A}\mathbf{U}.$$

Then we can define a new sample pair $(\hat{\mathbf{Y}}, \hat{\mathbf{\Omega}})$ for $\hat{\mathbf{A}}$ as

$$\hat{\mathbf{Y}} = \mathbf{L}\mathbf{Y}, \quad \hat{\mathbf{\Omega}} = \mathbf{U}^{-1}\mathbf{\Omega}.$$

That $(\hat{\mathbf{Y}}, \hat{\mathbf{\Omega}})$ is indeed a sample pair for $\hat{\mathbf{A}}$ follows directly from the calculation

$$\hat{\mathbf{Y}} = \mathbf{L}\mathbf{A}\mathbf{\Omega} = \mathbf{L}\mathbf{A}\mathbf{U}\mathbf{U}^{-1}\mathbf{\Omega} = \hat{\mathbf{A}}\hat{\mathbf{\Omega}}.$$

Observe that if \mathbf{L} and \mathbf{U} are well-conditioned and independent of the test matrix $\mathbf{\Omega}$, then the new sample pair $(\hat{\mathbf{Y}}, \hat{\mathbf{\Omega}})$ will provide a high-quality sketch of $\hat{\mathbf{A}}$. In the method described, the matrices \mathbf{L} and \mathbf{U} will not be entirely independent of $\mathbf{\Omega}$, but extensive numerical experiments indicate that the dependence is sufficiently weak that sketches remain accurate throughout the compression and factorization process. This principle underlies the **RSRS** algorithm: as we recursively apply structured factorizations to compress and invert \mathbf{A} , we update sketch matrices in tandem using transformations derived from the factorization itself, without ever needing direct access to matrix entries.

1.2. Outline of Paper. The manuscript is structured as follows: Section 2 reviews mathematical preliminaries of randomized linear algebra and sparse LU factorization. Section 3 describes LU factorizations of \mathcal{H}^2 -matrices under the strong admissibility condition, focusing on the case where matrix entries are available. Section 4 focuses on computing the invertible factorization when the matrix is accessible only through its action on vectors. Two key tools are introduced for efficiently computing low-rank factorizations of admissible sub-blocks and extracting dense sub-blocks using matrix-vector products. Finally, Section 5 presents numerical results for various discretizations and complex geometries in 2D and 3D, demonstrating the performance of **RSRS** in terms of speed, sample requirements, and accuracy.

2. PRELIMINARIES

We briefly summarize notation used throughout the paper. We use the notation \mathbf{l}, \mathbf{J} to denote vectors of indices. The notation $\mathbf{A}_{\mathbf{l}\mathbf{J}}$ denotes the sub-block of matrix \mathbf{A} corresponding to the set of row indices \mathbf{l} and the column indices \mathbf{J} . The Euclidean norm of a vector \mathbf{x} is $\|\mathbf{x}\|$ and for a given matrix \mathbf{A} , the induced operator norm (or ‘‘spectral norm’’) is $\|\mathbf{A}\|$. We also introduce some shorthands for linear algebraic operations on a matrix $\mathbf{A} \in \mathbb{R}^{m \times n}$. An orthonormal matrix $\mathbf{Q} \in \mathbb{R}^{m \times n}$ is a matrix such that $\|\mathbf{Q}\| = 1$ and $\mathbf{Q}^* \mathbf{Q} = \mathbf{I}$. For $m \geq n$, the operation

$$(3) \quad \text{orth}(\mathbf{A}) := \mathbf{Q} \in \mathbb{R}^{m \times n}$$

gives an orthonormal basis for the column space of \mathbf{A} such that $\mathbf{Q} \mathbf{Q}^* \mathbf{A} = \mathbf{A}$. The notation

$$(4) \quad \text{orth}_k(\mathbf{A}) := \mathbf{Q} \in \mathbb{R}^{m \times k}$$

gives an orthonormal basis for the space spanned by the dominant k left singular vectors of \mathbf{A} . For $m < n$, the operation

$$(5) \quad \text{null}(\mathbf{A}) := \mathbf{Q} \in \mathbb{R}^{n \times (n-m)}$$

gives an orthonormal basis for the nullspace of \mathbf{A} , so that $\|\mathbf{A} \mathbf{y}\| = 0$ for every vector \mathbf{y} in the range of $\text{null}(\mathbf{A})$. The dagger notation denotes the pseudoinverse, e.g. for $\mathbf{A} \in \mathbb{R}^{n \times m}$ where $m < n$, $\mathbf{A} \mathbf{A}^\dagger = \mathbf{I}$.

2.1. Randomized Low Rank Approximation. Suppose we would like to compute a low-rank approximation to the matrix $\mathbf{A} \in \mathbb{R}^{m \times n}$ of rank k , i.e. we would like to find an orthogonal matrix $\mathbf{Q} \in \mathbb{R}^{m \times k}$ and some matrix $\mathbf{B} \in \mathbb{R}^{k \times n}$ such that

$$(6) \quad \left\| \begin{array}{cc} \mathbf{A} & - \mathbf{Q} \mathbf{B} \\ m \times n & m \times k \quad k \times n \end{array} \right\| \quad \text{is small.}$$

This task can be accomplished with $(k+p)$ matrix-vector products of \mathbf{A} and its adjoint, where p is a small parameter, e.g. $p = 5$. First, generate a randomized sketch of the matrix \mathbf{A} as

$$(7) \quad \begin{array}{c} \mathbf{Y} \\ m \times (k+p) \end{array} = \begin{array}{cc} \mathbf{A} & \mathbf{\Omega} \\ m \times n & n \times (k+p) \end{array}, \quad \Omega_{ij} \sim \mathcal{N}(0, 1)$$

where the entries of $\mathbf{\Omega}$ are drawn from a Gaussian random distribution. With high probability, the columns of \mathbf{Y} span the dominant range of \mathbf{A} [37]. Then an approximate factorization of \mathbf{A} can be computed as

$$(8) \quad \begin{array}{c} \mathbf{Q} \\ m \times k \end{array} = \text{orth}_k(\mathbf{Y}), \quad \mathbf{B} := \mathbf{Q}^* \mathbf{A},$$

where the computation for \mathbf{B} is done by the action of the adjoint of \mathbf{A} . Though the computation involves randomization, the produced basis in (8) is within a polynomial factor of optimal. For $k \geq 2, p \geq 4$ and $k+p \leq \min(m, n)$, the probability that

$$(9) \quad \|\mathbf{A} - \mathbf{Q} \mathbf{Q}^* \mathbf{A}\| \leq \left(1 + 8\sqrt{(k+p)p \log p}\right) \sigma_k + 3 \sqrt{(k+p) \sum_{j>k} \sigma_j^2}$$

approaches 1 a rate faster than any exponential function with increasing p [25, Corollary 10.9]. For many PDE operators, where the singular values decay exponentially, the gap from optimality is essentially bounded by a polynomial factor that depends only on k and p . Randomized sketching methods can be used to construct a wide range of low-rank decompositions, including the interpolative decomposition of Section 2.3. These methods are especially useful in the black-box setting of (2) because the matrix \mathbf{A} is only accessed through its action on vectors.

2.2. Block elimination matrices. Consider a block matrix of the form

$$(10) \quad \mathbf{A} = \begin{pmatrix} \mathbf{A}_{11} & \mathbf{A}_{12} & \\ \mathbf{A}_{21} & \mathbf{A}_{22} & \mathbf{A}_{23} \\ & \mathbf{A}_{32} & \mathbf{A}_{33} \end{pmatrix}.$$

If \mathbf{A}_{11} is non-singular, we can “decouple” it from the other blocks via one step of block Gaussian elimination, by multiplying the \mathbf{A} on the left and right with matrices \mathbf{L} and \mathbf{U} as

$$(11) \quad \mathbf{L} \mathbf{A} \mathbf{U} = \begin{pmatrix} \mathbf{A}_{11} & & \\ & \mathbf{S}_{22} & \mathbf{A}_{23} \\ & & \mathbf{A}_{33} \end{pmatrix},$$

where the matrices \mathbf{L} and \mathbf{U} are unit-triangular matrices

$$(12) \quad \mathbf{L} = \begin{pmatrix} \mathbf{I} & & \\ -\mathbf{A}_{21}\mathbf{A}_{11}^{-1} & \mathbf{I} & \\ & & \mathbf{I} \end{pmatrix} \quad \text{and} \quad \mathbf{U} = \begin{pmatrix} \mathbf{I} & -\mathbf{A}_{11}^{-1}\mathbf{A}_{12} & \\ & \mathbf{I} & \\ & & \mathbf{I} \end{pmatrix},$$

and the submatrix \mathbf{S}_{22} in (11) is the Schur complement

$$(13) \quad \mathbf{S}_{22} = \mathbf{A}_{22} - \mathbf{A}_{21}\mathbf{A}_{11}^{-1}\mathbf{A}_{12}.$$

Block-elimination matrices of the form in (12) are simple to invert by toggling the sign of the off-diagonal block. When \mathbf{A} is symmetric, the factor $\mathbf{U} = \mathbf{L}^*$ and symmetry is preserved in (11).

2.3. The interpolative decomposition. Let $\mathbf{A}_{\mathbf{I}\mathbf{J}}$ be a matrix subblock of size $m \times n$ and approximate rank k . The *interpolative decomposition (ID)* of $\mathbf{A}_{\mathbf{I}\mathbf{J}}$ is a low rank factorization where a subset of k rows/columns is used to span the row/column space of \mathbf{A} . To be precise, for the *row ID*, we find a partition $\mathbf{I} = \mathbf{R} \cup \mathbf{S}$, such that the matrix admits a low rank decomposition

$$(14) \quad \mathbf{A}_{\mathbf{I}\mathbf{J}} = \begin{pmatrix} \mathbf{A}_{\mathbf{R}\mathbf{J}} \\ \mathbf{A}_{\mathbf{S}\mathbf{J}} \end{pmatrix} \approx \begin{pmatrix} \mathbf{T} \\ \mathbf{I} \\ \mathbf{I} \end{pmatrix} \begin{matrix} (m-k) \times k \\ k \times k \\ k \times n \end{matrix} \mathbf{A}_{\mathbf{S}\mathbf{J}}.$$

Finding the optimal k rows is a combinatorially hard problem. However, the strong rank-revealing QR factorization [23] is guaranteed to produce a near-optimal factorization. In practice, the standard pivoted QR with a greedy approach performs well. Although the error in an approximate low-rank k interpolative decomposition can, in theory, be significantly larger than that obtained by truncating a singular value decomposition, the practical error is usually modest when the singular values of the input matrix decay at a reasonable rate, as is often the case for PDE problems. For numerical stability, it is desirable that the matrix \mathbf{T} be well-conditioned, which in practice means keeping its entries small. It has been demonstrated that one can always choose the set \mathbf{S} such that every entry of \mathbf{T} has a modulus bounded by one, and practical algorithms exist to ensure that these entries remain modest [16, 23, 35].

In scenarios where the matrix is not easily accessible, randomized methods [18, 30, 36, 43] provide an efficient means of computing the skeleton set and the interpolation matrix \mathbf{T} . Suppose that one computes the ID of the sketch

$$(15) \quad \mathbf{Y}_{\mathbf{I}} = \begin{matrix} m \times (k+p) \\ \mathbf{A}_{\mathbf{I}\mathbf{J}} \\ n \times (k+p) \end{matrix} \mathbf{\Omega}, \quad \text{id}(\mathbf{Y}_{\mathbf{I}}) = \begin{matrix} \mathbf{R} \cup \mathbf{S} & \mathbf{T} \\ m-k & k & (m-k) \times k \end{matrix}.$$

Then, by some simple observations [37, Section 13.3], the information needed for the ID of $\mathbf{A}_{\mathbf{I}\mathbf{J}}$ is provided by the ID of the sketch $\mathbf{Y}_{\mathbf{I}}$. Because the sketch approximately spans the range of \mathbf{A} , the matrix admits the low rank decomposition

$$\mathbf{A}_{\mathbf{I}\mathbf{J}} \approx \begin{matrix} m \times n \\ \mathbf{Y}_{\mathbf{I}} \\ m \times (k+p) \end{matrix} \begin{matrix} \mathbf{B} \\ (k+p) \times n \end{matrix}$$

for some matrix \mathbf{B} . Consequently,

$$(16) \quad \begin{pmatrix} \mathbf{A}_{\text{RJ}} \\ \mathbf{A}_{\text{SJ}} \end{pmatrix} \approx \begin{pmatrix} \mathbf{Y}_{\text{R}} \\ \mathbf{Y}_{\text{S}} \end{pmatrix} \mathbf{B} \approx \begin{pmatrix} \mathbf{T} \\ \mathbf{I} \end{pmatrix} \mathbf{Y}_{\text{S}} \mathbf{B} = \begin{pmatrix} \mathbf{T} \\ \mathbf{I} \end{pmatrix} \mathbf{A}_{\text{SJ}}.$$

Thus, the key information needed for the ID of \mathbf{A}_{IJ} is encapsulated in the ID of the sketch \mathbf{Y}_{I} . Using deterministic methods, the complexity of the ID is $\mathcal{O}(mn^2)$. Randomized methods reduce the complexity to $\mathcal{O}(mnk + mk^2)$ when using Gaussian random matrices. Likewise, to compute a representative set of columns, the algorithm described can be executed by sketching the transpose of the matrix.

3. LU FACTORIZATION OF HIERARCHICAL MATRICES USING STRONG ADMISSIBILITY

In this section, we describe the construction of an invertible factorization for \mathcal{H}^2 matrices under the strong admissibility condition, largely following the presentation in [40]. As an example, consider the matrix \mathbf{A} defined by the Green's function G for the Laplace equation:

$$(17) \quad \begin{aligned} \mathbf{A}_{ij} &= G(\mathbf{x}_i, \mathbf{x}_j), \quad i \neq j \\ \text{where } G(\mathbf{x}_i, \mathbf{x}_j) &= \begin{cases} \log(\|\mathbf{x}_i - \mathbf{x}_j\|), & \mathbf{x} \in \mathbb{R}^2 \\ (\|\mathbf{x}_i - \mathbf{x}_j\|)^{-1}, & \mathbf{x} \in \mathbb{R}^3. \end{cases} \end{aligned}$$

An appropriate quadrature correction is applied on the diagonal to ensure that \mathbf{A} is invertible. Matrices of this type may arise from the discretization of an integral equation or from covariance matrices in statistics. For simplicity in this section, we assume that the matrix entries are readily accessible and that the matrix is stored densely. However, when \mathbf{A} originates from the discretization of an integral equation with an explicit formula for evaluating its entries, efficient algorithms that avoid forming the matrix densely are detailed in [40, 42].

The algorithms rely on organizing a set of points $\{\mathbf{x}_j\}_{j=1}^N$ into a hierarchical structure, either a quadtree in two dimensions or an octree in three dimensions, depending on whether the points lie in 2D or 3D space, respectively. Formally, we construct a tree \mathcal{T} in which each node, or box B , contains a subset of the points. Initially, all points are contained in a single box called the root. The root box is recursively subdivided into 2^d child boxes, where d is the dimension of the space. This subdivision continues until each box contains no more than a specified threshold number of points, m . We refer to a box that has children as a tree box, and a box with no children as a leaf. The depth of a box is its distance (in number of edges) from the root box. The collection of all boxes at depth ℓ is called level ℓ of the tree. Thus, level 0 consists of just the root box, level 1 contains its 2^d children, and higher levels correspond to progressively finer partitions of the domain. The depth of the tree, denoted L , is the maximum depth of any box, and is approximately given by $L \approx \log_2 \left(\frac{N}{m} \right)$.

Two boxes in the tree are said to be adjacent if they share a face, edge, or corner. In cases where the point distribution is non-uniform, only those boxes containing more than m points are further subdivided, resulting in an adaptive tree structure. We assume that such adaptive trees satisfy a 2:1 balance condition, meaning that any two adjacent leaf boxes differ in depth by at most one. This constraint limits the number of adjacent boxes and helps maintain computational efficiency. For a given box B , we distinguish between its neighbor boxes—those that are adjacent—and its far-field boxes—those that are well-separated. In a slight abuse of notation, we also use \mathbf{B} to denote the set of indices corresponding to points within box B . Similarly, \mathbf{N} refers to the indices of points in the neighboring boxes of B , while \mathbf{F} refers to the indices of points in its far-field boxes.

3.1. Strong Skeletonization. For a dense matrix \mathbf{A} , the procedure described in this section introduces and exploits sparsity in a modified system via a sequence of linear transformations applied

to \mathbf{A} . Assume that the matrix is tessellated according to the geometry, following the index order $[\mathbf{B}, \mathbf{N}, \mathbf{F}]$, so that

$$(18) \quad \mathbf{A} = \begin{pmatrix} \mathbf{A}_{\mathbf{BB}} & \mathbf{A}_{\mathbf{BN}} & \mathbf{A}_{\mathbf{BF}} \\ \mathbf{A}_{\mathbf{NB}} & \mathbf{A}_{\mathbf{NN}} & \mathbf{A}_{\mathbf{NF}} \\ \mathbf{A}_{\mathbf{FB}} & \mathbf{A}_{\mathbf{FN}} & \mathbf{A}_{\mathbf{FF}} \end{pmatrix}, \quad \text{where} \quad \begin{array}{l} \mathbf{B}: \text{target box indices for box } B, \\ \mathbf{N}: \text{near field indices,} \\ \mathbf{F}: \text{far field indices.} \end{array}$$

Consider the subblock $\mathbf{A}_{\mathbf{BF}}$ corresponding to the interaction between a box and its far field points. Because the points are well-separated, the matrix is low-rank and admits the interpolative decomposition of Section 2.3 as

$$(19) \quad \mathbf{B} = \begin{array}{c} \mathbf{R} \\ m \end{array} \cup \begin{array}{c} \mathbf{S} \\ m-k \\ k \end{array}, \quad (\mathbf{A}_{\mathbf{FR}} \quad \mathbf{A}_{\mathbf{FS}}) \approx \mathbf{A}_{\mathbf{FS}} \begin{pmatrix} \mathbf{T} & \mathbf{I} \\ (m-k) \times k & k \times k \end{pmatrix}.$$

Likewise, an analogous statement holds for $\mathbf{A}_{\mathbf{BF}}$. It is often convenient to choose a skeleton set and corresponding interpolation matrix which is applicable for both $\mathbf{A}_{\mathbf{BF}}$ and $\mathbf{A}_{\mathbf{FB}}$. This can be done by computing the ID of the concatenation so that

$$(20) \quad \begin{pmatrix} \mathbf{A}_{\mathbf{FR}} & \mathbf{A}_{\mathbf{FS}} \\ \mathbf{A}_{\mathbf{RF}}^* & \mathbf{A}_{\mathbf{SF}}^* \end{pmatrix} \approx \begin{pmatrix} \mathbf{A}_{\mathbf{FS}} \\ \mathbf{A}_{\mathbf{SF}}^* \end{pmatrix} (\mathbf{T} \quad \mathbf{I}).$$

Instead of using low-rank decompositions, which project onto a k -dimensional subspace, we aim to remain in the full m -dimensional space while introducing sparsity into the system. In this approach, an equivalent formulation of (19) is given by

$$(21) \quad (\mathbf{A}_{\mathbf{FR}} \quad \mathbf{A}_{\mathbf{FS}}) \begin{pmatrix} \mathbf{I} \\ -\mathbf{T} \quad \mathbf{I} \end{pmatrix} = (\mathbf{A}_{\mathbf{FR}} - \mathbf{A}_{\mathbf{FS}}\mathbf{T} \quad \mathbf{A}_{\mathbf{FS}}) \approx (\mathbf{0} \quad \mathbf{A}_{\mathbf{FS}}).$$

For an appropriate permutation $[\mathbf{R}, \mathbf{S}, \mathbf{N}, \mathbf{F}]$, we define sparsifying matrices \mathbf{E}, \mathbf{F} which operate on the full $N \times N$ matrix as follows:

$$(22) \quad \mathbf{E} = \left(\begin{array}{cc|c} \mathbf{I} & -\mathbf{T}^* & \\ & \mathbf{I} & \\ \hline & & \mathbf{I} \\ & & \mathbf{I} \end{array} \right), \quad \mathbf{F} = \left(\begin{array}{cc|c} \mathbf{I} & & \\ -\mathbf{T} & \mathbf{I} & \\ \hline & & \mathbf{I} \\ & & \mathbf{I} \end{array} \right).$$

Applying \mathbf{E} and \mathbf{F} to the left and right of \mathbf{A} gives the sparsified system

$$(23) \quad \mathbf{E} \mathbf{A} \mathbf{F} \approx \begin{pmatrix} \mathbf{X}_{\mathbf{RR}} & \mathbf{X}_{\mathbf{RS}} & \mathbf{X}_{\mathbf{RN}} & \\ \mathbf{X}_{\mathbf{SR}} & \mathbf{A}_{\mathbf{SS}} & \mathbf{A}_{\mathbf{SN}} & \mathbf{A}_{\mathbf{SF}} \\ \mathbf{X}_{\mathbf{NR}} & \mathbf{A}_{\mathbf{NS}} & \mathbf{A}_{\mathbf{NN}} & \mathbf{A}_{\mathbf{NF}} \\ & \mathbf{A}_{\mathbf{FS}} & \mathbf{A}_{\mathbf{FN}} & \mathbf{A}_{\mathbf{FF}} \end{pmatrix}.$$

The interactions between \mathbf{R} and the far field \mathbf{F} become approximately zero. Importantly, the use of the ID does not modify any entries associated with the skeleton subset \mathbf{S} , thereby preserving a physical interpretation of the system. This retention of structure enables the application of analytic compression techniques, such as proxy surfaces [47, 48] or adaptive cross-approximation [7, 11, 20] for discretized boundary integral equations. Now that the matrix is sparser, the objective is to *diagonalize* the interactions between the redundant box indices \mathbf{R} and the remaining indices of the matrix (i.e., to eliminate the residual sparse interactions). This can be achieved using standard sparse block-elimination techniques, as described in Section 2.2. We introduce matrices \mathbf{L}, \mathbf{U} as

$$(24) \quad \mathbf{L} = \left(\begin{array}{cc|c} \mathbf{I} & & \\ -\mathbf{X}_{\mathbf{SR}}\mathbf{X}_{\mathbf{RR}}^{-1} & \mathbf{I} & \\ -\mathbf{X}_{\mathbf{NR}}\mathbf{X}_{\mathbf{RR}}^{-1} & & \mathbf{I} \\ \hline & & \mathbf{I} \end{array} \right), \quad \mathbf{U} = \left(\begin{array}{cc|c} \mathbf{I} & -\mathbf{X}_{\mathbf{RR}}^{-1}\mathbf{X}_{\mathbf{RS}} & -\mathbf{X}_{\mathbf{RR}}^{-1}\mathbf{X}_{\mathbf{RN}} \\ & \mathbf{I} & \\ \hline & & \mathbf{I} \\ & & \mathbf{I} \end{array} \right).$$

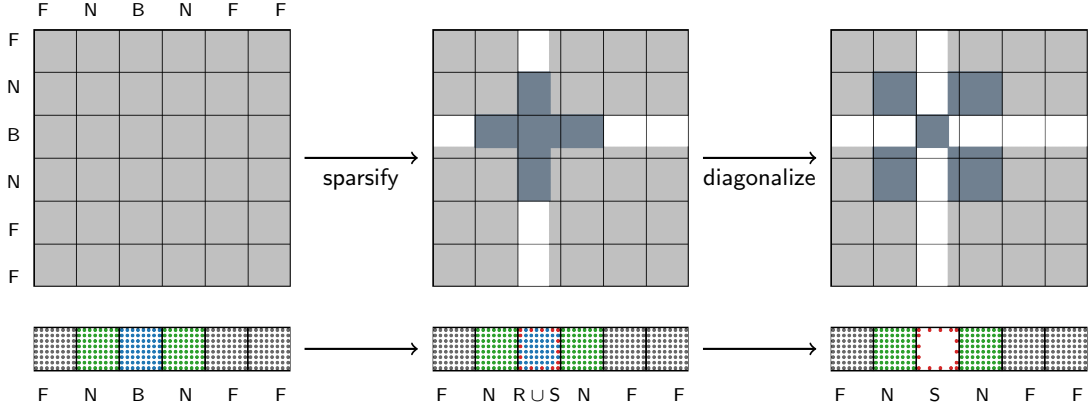


FIGURE 1. On the top row, there is a pseudo-one dimensional domain, where each box has a neighbor on the left and the right. In order to diagonalize a subset of indices of Box 1, the procedure is first to identify “redundant” indices according to the ID, to sparsify the matrix. Then, the sparse interactions are diagonalized using sparse block elimination matrices. At each stage, the corresponding sparsity pattern of the matrix is shown, with modified entries in red.

Then applying \mathbf{L} and \mathbf{U} to the left and right, respectively, yields the diagonalized matrix $\tilde{\mathbf{A}}$

$$(25) \quad \tilde{\mathbf{A}}(\mathbf{A}; B) = \mathbf{L} (\mathbf{E} \mathbf{A} \mathbf{F}) \mathbf{U} \approx \left(\begin{array}{c|cc} \mathbf{X}_{RR} & & \\ \hline \mathbf{X}_{SS} & \mathbf{X}_{SN} & \mathbf{A}_{SF} \\ \mathbf{X}_{NS} & \mathbf{X}_{NN} & \mathbf{A}_{NF} \\ \mathbf{A}_{FS} & \mathbf{A}_{FN} & \mathbf{A}_{FF} \end{array} \right),$$

where modifications to the original matrix entries are introduced to the near-neighbor interactions. We define *diagonalization* operators for a box B as \mathbf{V}, \mathbf{W} , which are compositions of the skeletonization and block-elimination operators:

$$(26) \quad \begin{aligned} \mathbf{V}^{-1} &= \mathbf{L} \mathbf{E}, \\ \mathbf{W}^{-1} &= \mathbf{F} \mathbf{U}, \quad \text{so that} \end{aligned}$$

$$\tilde{\mathbf{A}}(\mathbf{A}; B) \approx \mathbf{V}^{-1} \mathbf{A} \mathbf{W}^{-1} \quad \text{is diagonalized for } R \subseteq B \text{ for box } B.$$

Because the operators \mathbf{V}, \mathbf{W} are invertible, we can also express the decomposition as a sparse factorization of \mathbf{A} :

$$(27) \quad \mathbf{A} \approx \mathbf{V} \tilde{\mathbf{A}} \mathbf{W}.$$

The basic idea of the subsequent algorithmic steps is to repeat the sparsify-then-eliminate procedure for every box in the hierarchical tree decomposition. Because the interactions with respect to R have been diagonalized, these subsequent linear operations do not introduce additional nonzero interactions for R . We make two important remarks regarding the diagonalized matrix.

Remark 1. *Applying the sparsifying operators \mathbf{E} and \mathbf{F} on the left and right does modify the condition number of the subblock \mathbf{X}_{RR} , however, the effect is modest. In fact, owing to the bounded entries of \mathbf{T} (as discussed in Section 2.3), both \mathbf{E} and \mathbf{F} remain well-conditioned, and the condition number of \mathbf{A}_{RR} and that of the modified subblock exhibit only minor differences in practice.*

Remark 2. The diagonalized matrix $\tilde{\mathbf{A}}$ introduces an additive term of dense interactions between the near-neighbors \mathbf{N} , namely,

$$\mathbf{X}_{\mathbf{NN}} = \mathbf{A}_{\mathbf{NN}} - \mathbf{X}_{\mathbf{NR}}\mathbf{X}_{\mathbf{RR}}^{-1}\mathbf{X}_{\mathbf{RN}}.$$

Consider two boxes, α, β which neighbor B . Although α, β have a common neighbor, they may in fact be in each other's far field. For a concrete example, see Figure 1. Therefore, this additional term could in principle impact the existing low-rank spectrum. In practice, however, the modified interactions remain compressible as low rank. In settings where the matrix entries are explicitly accessible, these modified entries are stored in an intermediate representation and then recompressed in later stages of the algorithm.

3.2. Strong Recursive Skeletonization. In this section, we describe a recursive algorithm by composing the diagonalization operators defined in Section 3.1. First, we describe how the operators are composed for all the leaf boxes (e.g. containing at most m points). Then, we generalize to a multilevel decomposition on \mathcal{T} . Recall that the root box containing all the points is on level 0 and that the levels are labeled by their depth (e.g. the distance from the root), so the finest level is labeled L . Following the previous works [40, 42], the boxes are labeled B_1, B_2, \dots according to the order in which they are diagonalized.

Suppose that for leaf box B_1 on level L that we compute diagonalization operators $\mathbf{V}_1, \mathbf{W}_1$ so that a subset of indices $\mathbf{R}_1 \subseteq \mathbf{B}_1$ are diagonalized and decoupled from the rest of the dense system as

$$(28) \quad \tilde{\mathbf{A}}(\mathbf{A}; B_1) \approx \mathbf{V}_1^{-1} \mathbf{A} \mathbf{W}_1^{-1}.$$

The subsequent steps compute diagonalization operators for each box on level L ; however, there is an important caveat in Remark 2 that additive terms are introduced into the system, and the next computation needs to compute operators which diagonalize the modified system $\tilde{\mathbf{A}}$. Continuing this procedure, we maintain the modified matrix $\tilde{\mathbf{A}}(\mathbf{A}; B_1, B_2)$ and compute operators which will decouple $\mathbf{R}_2 \subseteq \mathbf{B}_2$ as

$$(29) \quad \tilde{\mathbf{A}}(\mathbf{A}; B_1, B_2) = \mathbf{V}_2^{-1} \tilde{\mathbf{A}}(\mathbf{A}; B_1) \mathbf{W}_2^{-1}.$$

Importantly, the operators $\mathbf{V}_2^{-1}, \mathbf{W}_2^{-1}$ do not affect previously diagonalized indices, and the redundant indices $\mathbf{R}_1 \subseteq \mathbf{B}_1$ remain diagonalized. A uniform tree in d dimensions has 2^L leaf boxes. After diagonalizing these boxes, the sparsified matrix takes the form

$$(30) \quad \tilde{\mathbf{A}}(\mathbf{A}; B_1, \dots, B_{2^L}) = \mathbf{V}_{2^d}^{-1} \dots \mathbf{V}_1^{-1} \mathbf{A} \mathbf{W}_1^{-1} \dots \mathbf{W}_{2^L}^{-1},$$

where $\mathbf{R}_1, \dots, \mathbf{R}_{2^L}$ are diagonalized. See the top row of Figure 2 for a visualization of a pseudo-one dimensional domain with 8 leaf boxes.

To continue strong recursive skeletonization, we now need to regroup the remaining skeleton indices, according to a coarser level of the tree. The interactions between target boxes and the far-field on the coarser level are also low rank, and can be sparsified then diagonalized using the methodology introduced in Section 3.1. We introduce notation for the remaining *active* set of points, which we update after diagonalizing indices $\mathbf{R}_1, \dots, \mathbf{R}_j$,

$$(31) \quad \text{active} = [1, \dots, N] \setminus (\mathbf{R}_1 \cup \dots \cup \mathbf{R}_j)$$

as well as corresponding notation for the remaining *active* box and neighbor points for a box B

$$(32) \quad \mathbf{B}_{\text{active}} = \mathbf{B} \cap \text{active}, \quad \mathbf{N}_{\text{active}} = \mathbf{N} \cap \text{active}.$$

In computing diagonalization operators $\mathbf{V}^{-1}, \mathbf{W}^{-1}$, only the remaining ‘‘active’’ indices enter into the computation.

In the setting where matrix-entries are available, the modified entries of the matrix are stored explicitly, and the unmodified entries can be computed as needed. As we noted in Remark 2, strong recursive skeletonization introduces additive terms between boxes which are well-separated.

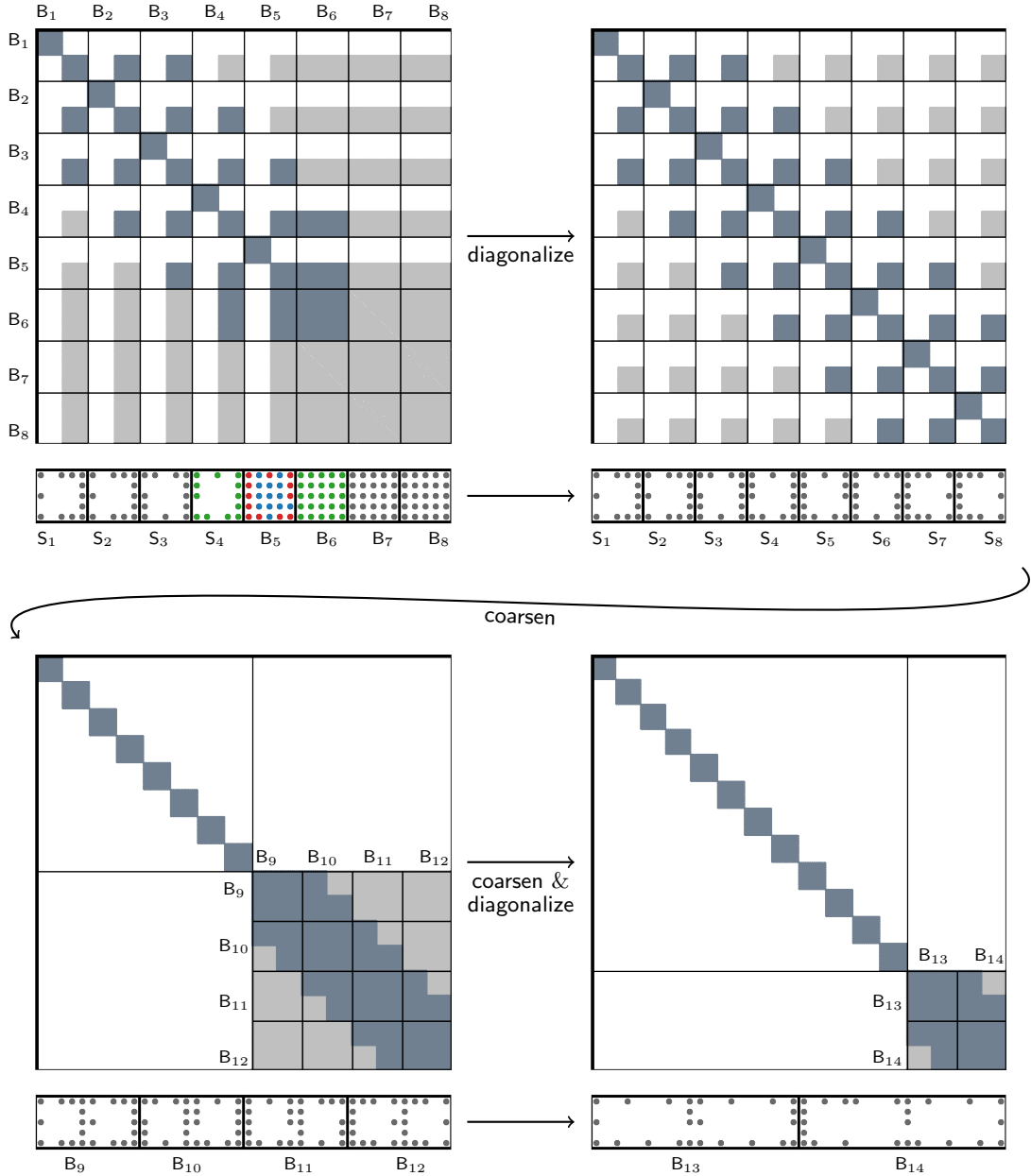


FIGURE 2. For a pseudo-one dimensional geometry, the active points as well as the corresponding matrix are shown at various stages of the computation. First, the redundant points of the boxes on the finest level are diagonalized. To continue the computation, the remaining active points are regrouped (according to the next coarse level of the tree), which introduces low rank subblocks which can be sparsified.

In subsequent steps, these additive terms need to be recompressed as low rank. In computing the ID for the subblock $\tilde{\mathbf{A}}_{B_{\text{active}}F}$, the modified entries need to be compressed algebraically, whereas the unmodified entries can be compressed using analytic techniques (e.g. proxy surfaces or adaptive cross approximation). The modified entries in the far-field are localized, and efficient methods to handle the compression accurately are detailed in [42]. For geometries in 2D and 3D, there are far

more modified pairwise interactions between boxes, as demonstrated in Figure 3, which need to be stored and recompressed.

To formalize the description of recursive skeletonization with strong admissibility, consider that the boxes are diagonalized in an upward traversal through the tree in order $1, \dots, M$, terminating at box B_M . Let the index vector B_t denote the remaining active points in the domain at the time the algorithm terminates and the permutation vector P_t order the points in the order that they have been eliminated. We define the remaining dense active submatrix by extracting subindices

$$(33) \quad \tilde{\mathbf{A}}_{B_t B_t}, \quad \text{where} \quad \tilde{\mathbf{A}} = \tilde{\mathbf{A}}(\mathbf{A}; B_1, \dots, B_M).$$

The full diagonalized matrix takes the form

$$(34) \quad \mathbf{P}_t \mathbf{D} \mathbf{P}_t^T = \mathbf{P}_t \begin{pmatrix} \mathbf{X}_{R_1 R_1} & & & \\ & \ddots & & \\ & & \mathbf{X}_{R_M R_M} & \\ & & & \tilde{\mathbf{A}}_{B_t B_t} \end{pmatrix} \mathbf{P}_t^T \\ = \tilde{\mathbf{A}}(\mathbf{A}; B_1, \dots, B_M) \approx \mathbf{V}_M^{-1} \dots \mathbf{V}_1^{-1} \mathbf{A} \mathbf{W}_1^{-1} \dots \mathbf{W}_M^{-1}$$

The diagonalized system (34) leads to a sparse factorization of \mathbf{A} , as well as an equation for the inverse because each of the diagonalization operators is a composition of sparse invertible operators

$$(35) \quad \mathbf{A} \approx \mathbf{V}_1 \dots \mathbf{V}_M \mathbf{P}_t \mathbf{D} \mathbf{P}_t^T \mathbf{W}_M \dots \mathbf{W}_1,$$

$$(36) \quad \mathbf{A}^{-1} \approx \underbrace{\mathbf{W}_1^{-1} \dots \mathbf{W}_M^{-1}}_{\text{downward pass}} \mathbf{P}_t \mathbf{D}^{-1} \mathbf{P}_t^T \underbrace{\mathbf{V}_M^{-1} \dots \mathbf{V}_1^{-1}}_{\text{upward pass}}.$$

For symmetric positive definite matrices, the diagonalization operators \mathbf{V}, \mathbf{W} are symmetric as well, and the factorization (35) can be used to compute the square root $\sqrt{\mathbf{A}}$.

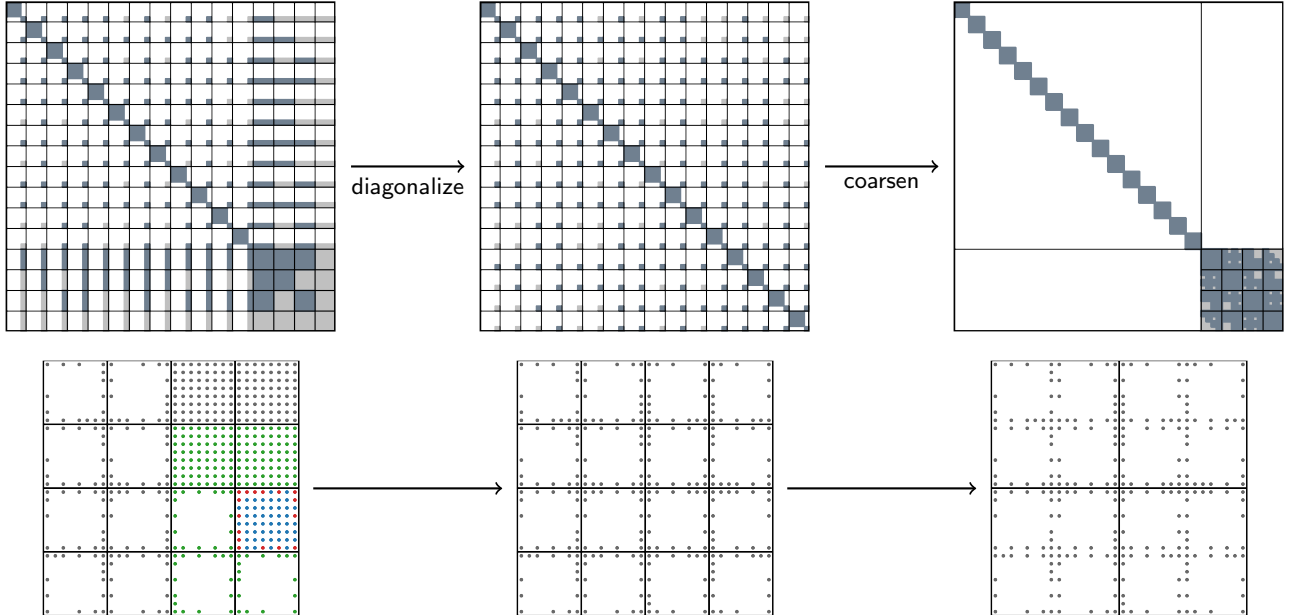


FIGURE 3. The analog of Figure 2 when the computational domain is a unit box. Observe that many more blocks get updated for a true two-dimensional domain. For every diagonalization step, up to 35 pairwise interactions are introduced between non-neighboring boxes, which need to be stored and later recompressed.

4. RANDOMIZED COMPRESSION AND LU FACTORIZATION USING SKETCHING

In this section, we describe randomized methods for recovering an invertible factorization of \mathbf{A} , as defined in Section 3, in settings where direct access to matrix entries is prohibitively expensive. Instead, we assume that \mathbf{A} is accessible only through matrix-vector products with \mathbf{A} and its adjoint \mathbf{A}^* . The factorization is reconstructed from random sketches of the form

$$(37) \quad \mathbf{Y} = \mathbf{A} \mathbf{\Omega}, \quad \mathbf{Z} = \mathbf{A}^* \mathbf{\Psi}, \quad \mathbf{\Omega}, \mathbf{\Psi} \sim \mathcal{N}(\mathbf{0}, \mathbf{I}),$$

$N \times s$ $N \times N N \times s$ $N \times s$ $N \times N N \times s$

by postprocessing the set $\{\mathbf{Y}, \mathbf{\Omega}, \mathbf{Z}, \mathbf{\Psi}\}$. We defer discussion of the required sample size s to later sections, but for now assume $s \ll N$. Recall from Section 3.1 that diagonalizing a set of indices $\mathbf{R} \subseteq \mathbf{B}$ proceeds by first compressing interactions between a target box and its far field, followed by extracting the remaining near-field (inadmissible) sub-blocks between \mathbf{R} and neighboring indices \mathbf{N} .

A natural strategy for performing these operations within the randomized sketching framework is to design *structured* test matrices $\mathbf{\Omega}, \mathbf{\Psi}$ containing zero or identity sub-blocks. For example, zeroing out the near-field sub-blocks isolates far-field interactions $\mathbf{A}_{\mathbf{BF}}$, while placing identity blocks on the near field can directly extract sparsified near-field interactions. However, constructing such structured test matrices poses significant challenges. First, they typically require substantially larger sample sizes to ensure accurate recovery. Second, and more fundamentally, the skeleton indices are computed dynamically during factorization (due to recompressions discussed in Section 3), making it impractical to design structured test matrices in advance.

Instead, we adopt a more flexible approach: we begin with dense Gaussian test matrices $\mathbf{\Omega}, \mathbf{\Psi}$ and impose the necessary structure *as needed* during the algorithm via linear transformations. This strategy preserves the generality of randomized sketching while enabling both far-field compression and near-field extraction. Our approach builds on techniques introduced in [28], trading modest post-processing overhead for a substantial reduction in the number of required samples.

Block Nullification: Applies a linear transformation to a Gaussian test matrix $\mathbf{\Omega}$ to produce a modified matrix $\mathbf{\Omega}'$, where the contribution of the near field has been “nullified.” This enables efficient sampling of far-field interactions $\mathbf{A}_{\mathbf{BF}}$. See Figure 4a for an illustration of $\mathbf{\Omega}'$.

Block Extraction: Applies a linear transformation to a Gaussian test matrix $\mathbf{\Omega}$ to produce a modified matrix $\mathbf{\Omega}'$ that “extracts” specific sub-blocks of a sparse matrix. This allows near-field sub-blocks to be extracted without prior knowledge of their locations. See Figure 4b for an illustration of $\mathbf{\Omega}'$.

4.1. Block Nullification. Suppose we would like to compute the interpolative decomposition of the interactions between box indices \mathbf{B} and far field indices \mathbf{F} so that (20) holds. To accomplish this using the randomized sketching (as discussed in Section 2.3), we need to generate and postprocess the sketches

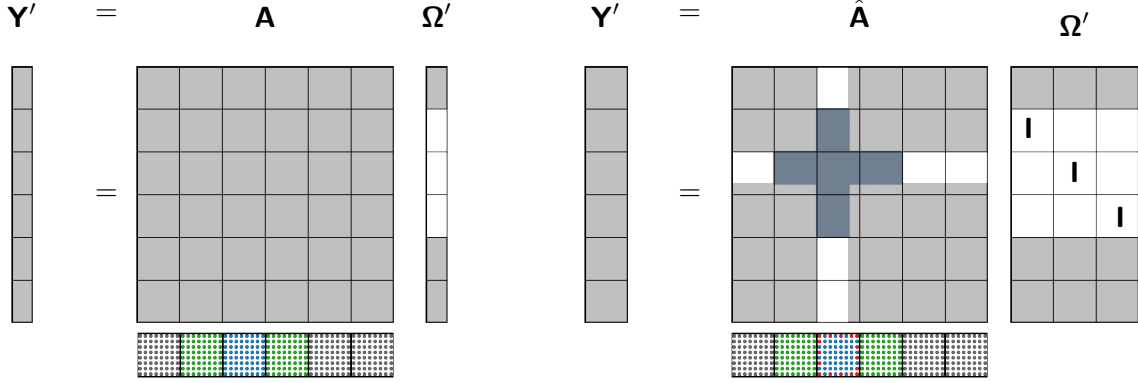
$$(38) \quad \mathbf{Y}'_{\mathbf{B}} = \mathbf{A}_{\mathbf{BF}} \mathbf{\Omega}'_{\mathbf{F}}, \quad \mathbf{Z}'_{\mathbf{B}} = \mathbf{A}_{\mathbf{FB}}^* \mathbf{\Psi}'_{\mathbf{F}},$$

where $\mathbf{\Omega}'_{\mathbf{F}}$ and $\mathbf{\Psi}'_{\mathbf{F}}$ are Gaussian random matrices.

For concreteness, suppose that each of the blocks in the tessellation are of size at most m , and the test and sketch matrices be tessellated according to the decomposition in Figure 4a. The matrix \mathbf{A} has full rank interactions between the target box and near-field boxes, complicating the straightforward use of randomized sketching. Ideally, the test matrices should reflect the sparsity pattern of the low-rank blocks we aim to sample. Consider a *structured* test matrix that, under an appropriate permutation $[\mathbf{B}, \mathbf{N}, \mathbf{F}]$, is designed to isolate the far-field interactions $\mathbf{A}_{\mathbf{BF}}$:

$$(39) \quad \mathbf{Y}'_{N \times (k+p)} = \mathbf{A}_{N \times N} \mathbf{\Omega}'_{N \times (k+p)}, \quad \text{where } \mathbf{\Omega}' = \begin{pmatrix} \mathbf{0}_{\mathbf{B}} \\ \mathbf{0}_{\mathbf{N}} \\ \mathbf{\Omega}'_{\mathbf{F}} \end{pmatrix}$$

Then, extracting the sub-block $\mathbf{Y}'_{\mathbf{B}}$ yields the required sketch in (38).



(A) Setting for block nullification.

(B) Setting for block extraction.

FIGURE 4. Two types of test matrices are needed for RSRs. (a) To sketch far-field interactions between a box and its distant neighbors. (b) To extract near-field interactions between a subset of box points and neighboring points. Rather than designing structured test matrices directly, we apply *block nullification* and *block extraction*, which use linear transformations of dense Gaussian matrices to introduce the desired structure.

Block nullification achieves the same objective without explicitly constructing a sparse test matrix. Instead, we apply a linear transformation to a dense Gaussian matrix Ω to produce a modified test matrix Ω' with desired zero sub-blocks. Specifically, given $\Omega \in \mathbb{R}^{N \times s}$ drawn from a Gaussian distribution, we compute a nullspace basis that annihilates the contributions of B and N , resulting in the desired test matrix

$$(40) \quad \begin{matrix} \Omega' \\ N \times (k+p) \end{matrix} = \begin{matrix} \Omega \\ N \times s \end{matrix} \begin{matrix} \mathbf{N}' \\ s \times (k+p) \end{matrix}, \quad \text{where } \mathbf{N}' = \text{null} \begin{pmatrix} \Omega_B \\ \Omega_N \end{pmatrix},$$

for a sufficient number of samples $s \geq |B| + |N| + k + p$.

Moreover, since we already have a sketch of \mathbf{A} as in (37), we do not need to explicitly form Ω' . Instead, we can apply the nullspace basis \mathbf{N}' directly to the extracted block:

$$(41) \quad \mathbf{Y}'_B = \underbrace{\mathbf{A}_{B,:} \Omega'}_{\text{extract B from (39)}} = \mathbf{A}_{B,:} \underbrace{\Omega \mathbf{N}'}_{\text{using (40)}} = \underbrace{\mathbf{A}_{B,:} \Omega}_{\text{extract B from (37)}} \mathbf{N}' = \mathbf{Y}_B \mathbf{N}' \quad \begin{matrix} m \times s & s \times (k+p) \end{matrix}$$

The cost of post-processing sketches using block nullification is $\mathcal{O}(m^3)$, with a constant depending on the number of neighboring blocks. Importantly, because the nullspace basis \mathbf{N}' is orthogonal, block nullification preserves the spectral properties of the original test matrix.

4.2. Block Extraction. In addition to sketching low-rank factors, we also need to extract the interactions between a target box and its near-field neighbors. In the factorization described in Section 3, the exact indices that need to be extracted are not known a priori — they are determined dynamically over the course of the algorithm, depending on which indices are selected as skeletons. Designing structured test matrices to extract these sub-blocks directly would both increase the sample complexity and require additional sketching operations as the algorithm proceeds. Instead, block extraction is similar in spirit to block nullification and applies a linear transformation to a dense Gaussian test matrix Ω to introduce structure into the test matrix *as needed* during post-processing.

Suppose that the matrix \mathbf{A} is partitioned according to $[B, N, F]$, and that for a subset $R \subseteq B$, the interactions with the far field satisfy $\mathbf{A}_{RF} \approx \mathbf{0}$. Our goal is to recover the remaining dense sub-block

\mathbf{A}_{RN} . A natural approach is to construct a *structured* test matrix that directly enables extracting \mathbf{A}_{RN} . Define $\mathbf{\Omega}'$ and its corresponding sketch \mathbf{Y}' as:

$$(42) \quad \mathbf{Y}'_{N \times l} = \mathbf{A}_{N \times N} \mathbf{\Omega}'_{N \times l}, \quad \text{where } \mathbf{\Omega}' = \begin{pmatrix} \mathbf{I}_{\text{B}} & \\ & \mathbf{I}_{\text{N}} \\ & & \mathbf{\Omega}'_{\text{F}} \end{pmatrix}, \quad l = |\text{B}| + |\text{N}|.$$

Extracting \mathbf{Y}'_{R} from this sketch directly yields the desired sub-block.

Rather than constructing $\mathbf{\Omega}'$ explicitly, we can compute it implicitly by applying a pseudoinverse transformation to the sub-blocks of a dense Gaussian matrix $\mathbf{\Omega} \in \mathbb{R}^{N \times s}$. Specifically:

$$(43) \quad \mathbf{\Omega}'_{N \times l} = \mathbf{\Omega}_{N \times s} \mathbf{P}'_{s \times l}, \quad \text{where } \mathbf{P}' = \begin{pmatrix} \mathbf{\Omega}_{\text{B}} \\ \mathbf{\Omega}_{\text{N}} \end{pmatrix}^{\dagger},$$

for $s > |\text{B}| + |\text{N}|$. Since we have already drawn a sketch of \mathbf{A} as in (37), we can apply \mathbf{P}' directly to a small extracted sub-block without forming $\mathbf{\Omega}'$ explicitly by following a similar procedure to (41):

$$(44) \quad (\mathbf{A}_{\text{RB}} \quad \mathbf{A}_{\text{RN}}) = \underbrace{\mathbf{A}_{\text{R},:} \mathbf{\Omega}'}_{\text{extract from (42)}} = \mathbf{A}_{\text{R},:} \underbrace{\mathbf{\Omega} \mathbf{P}'}_{\text{using (43)}} = \underbrace{\mathbf{A}_{\text{R},:} \mathbf{\Omega}}_{\text{extract from (37)}} \mathbf{P}' = \mathbf{Y}_{\text{R}} \mathbf{P}'.$$

The cost of post-processing the sketches using block extraction is $\mathcal{O}(m^3)$, with a constant depending on the number of neighboring blocks. Although the resulting entries $\mathbf{\Omega}'_{\text{F}}$ are no longer Gaussian, this does not substantially affect the accuracy of extracting sparse blocks, since these entries are multiplied against near-zero components of \mathbf{A} .

4.3. Randomized Strong Skeletonization. In Section 3.1, we described how to construct diagonalization operators that decouple a subset of box indices $\text{R} \subseteq \text{B}$ from their far field F , in settings where matrix entries are easily accessible. We now extend this approach to the setting where the matrix is only accessible through its action on vectors, using the techniques of block nullification and block extraction introduced in Sections 4.1 and 4.2. Suppose we have drawn sketches of \mathbf{A} and its adjoint as in (37), using s Gaussian random test vectors.

The first step is to construct sparsification operators \mathbf{E} and \mathbf{F} by computing an interpolation matrix \mathbf{T} and partitioning indices $\text{R} \cup \text{S} = \text{B}$, such that (20) holds. This is accomplished by computing an interpolative decomposition (ID) of the combined sketch:

$$(45) \quad [\text{R} \cup \text{S}, \mathbf{T}] = \text{id}(\mathbf{Y}'_{\text{B}} + \mathbf{Z}'_{\text{B}}), \quad \text{where } \mathbf{Y}'_{\text{B}} = \mathbf{A}_{\text{BF}} \mathbf{\Omega}'_{\text{F}}, \quad \mathbf{Z}'_{\text{B}} = \mathbf{A}_{\text{FB}}^* \mathbf{\Psi}'_{\text{F}}$$

with $\mathbf{\Omega}'_{\text{F}}, \mathbf{\Psi}'_{\text{F}}$ Gaussian random matrices. Rather than explicitly constructing these structured test matrices, block nullification allows us to compute the required sketches by post-processing the original sketches from (37):

$$(46) \quad \mathbf{Y}'_{\text{B}} = \mathbf{Y}_{\text{B}} \text{null} \begin{pmatrix} \mathbf{\Omega}_{\text{B}} \\ \mathbf{\Omega}_{\text{N}} \end{pmatrix}, \quad \mathbf{Z}'_{\text{B}} = \mathbf{Z}_{\text{B}} \text{null} \begin{pmatrix} \mathbf{\Psi}_{\text{B}} \\ \mathbf{\Psi}_{\text{N}} \end{pmatrix}$$

for $s \geq |\text{B}| + |\text{N}| + k + p$.

Next, to compute the sparse elimination operators \mathbf{L} and \mathbf{U} , we need to extract sparse sub-blocks, such as \mathbf{X}_{RN} and \mathbf{X}_{NR} . In order to accomplish this efficiently, we would like to sketch the sparsified system (22), where the interaction between R and F is approximately zero. We aim to generate sketches of the sparsified matrix by reusing the original sketches of \mathbf{A} . This is achieved using the fact that \mathbf{E} and \mathbf{F} are invertible. Specifically, for an appropriate permutation:

$$(47) \quad \mathbf{A} \approx \mathbf{E}^{-1} \begin{pmatrix} \mathbf{X}_{\text{RR}} & \mathbf{X}_{\text{RS}} & \mathbf{X}_{\text{RN}} & \\ \mathbf{X}_{\text{SR}} & \mathbf{A}_{\text{SS}} & \mathbf{A}_{\text{SN}} & \mathbf{A}_{\text{SF}} \\ \mathbf{X}_{\text{NR}} & \mathbf{A}_{\text{NS}} & \mathbf{A}_{\text{NN}} & \mathbf{A}_{\text{NF}} \\ & \mathbf{A}_{\text{FS}} & \mathbf{A}_{\text{FN}} & \mathbf{A}_{\text{FF}} \end{pmatrix} \mathbf{F}^{-1} := \mathbf{E}^{-1} \hat{\mathbf{A}} \mathbf{F}^{-1}.$$

Thus, we can obtain sketches of $\hat{\mathbf{A}}$ from the original sketches (37) by applying the following updates:

$$(48) \quad \hat{\mathbf{Y}} := \underbrace{\mathbf{E} \mathbf{Y}}_{\text{modified sketch matrix}} = \mathbf{E} \mathbf{A} \mathbf{\Omega} = \hat{\mathbf{A}} \underbrace{\mathbf{F}^{-1} \mathbf{\Omega}}_{\text{modified test matrix}} = \{\text{Set } \hat{\mathbf{\Omega}} := \mathbf{F}^{-1} \mathbf{\Omega}\} = \hat{\mathbf{A}} \hat{\mathbf{\Omega}}.$$

Likewise, the sketch of the adjoint can be updated as $\hat{\mathbf{Z}} := \mathbf{F}^* \mathbf{Z}$, $\hat{\mathbf{\Psi}} := \mathbf{E}^{-*} \mathbf{\Psi}$. Although the test matrices are modified and are no longer Gaussian, the modifications are sparse, and the matrices \mathbf{E} , \mathbf{F} are well-conditioned and do not significantly bias the test matrices. Now that sketches of $\hat{\mathbf{A}}$ have been obtained, block extraction can be used to compute

$$(49) \quad (\mathbf{X}_{RR} \quad \mathbf{X}_{RS} \quad \mathbf{X}_{RN}) \approx \hat{\mathbf{Y}}_R \begin{pmatrix} \hat{\mathbf{\Omega}}_B \\ \hat{\mathbf{\Omega}}_N \end{pmatrix}^\dagger, \quad (\mathbf{X}_{RR}^* \quad \mathbf{X}_{SR}^* \quad \mathbf{X}_{NR}^*) \approx \hat{\mathbf{Z}}_R \begin{pmatrix} \hat{\mathbf{\Psi}}_B \\ \hat{\mathbf{\Psi}}_N \end{pmatrix}^\dagger.$$

Here, approximate equalities are introduced because entries $\hat{\mathbf{A}}_{RF}$ are only approximately zero, and their contribution is added to the extracted subblocks.

Finally, we update the original sketch and test matrices to maintain sketches of the diagonalized matrix $\tilde{\mathbf{A}}$ for the subsequent steps of the algorithm, using the formula

$$(50) \quad \mathbf{A} \approx \mathbf{V} \left(\begin{array}{c|ccc} \mathbf{X}_{RR} & & & \\ \hline & \mathbf{X}_{SS} & \mathbf{X}_{SN} & \mathbf{A}_{SF} \\ & \mathbf{X}_{NS} & \mathbf{X}_{NN} & \mathbf{A}_{NF} \\ & \mathbf{A}_{FS} & \mathbf{A}_{FN} & \mathbf{A}_{FF} \end{array} \right) \mathbf{W} := \mathbf{V} \tilde{\mathbf{A}} \mathbf{W}.$$

Then, the following updates give a sketch of $\tilde{\mathbf{A}}$

$$(51) \quad \tilde{\mathbf{Y}} := \underbrace{\mathbf{V}^{-1} \mathbf{Y}}_{\text{modified sketch matrix}} = \mathbf{V}^{-1} \mathbf{A} \mathbf{\Omega} = \tilde{\mathbf{A}} \underbrace{\mathbf{W} \mathbf{\Omega}}_{\text{modified test matrix}} = \{\text{Set } \tilde{\mathbf{\Omega}} := \mathbf{W} \mathbf{\Omega}\} = \tilde{\mathbf{A}} \tilde{\mathbf{\Omega}}.$$

Likewise, the sketch of the adjoint can be updated as $\tilde{\mathbf{Z}} := \mathbf{W}^{-*} \mathbf{Z}$, $\tilde{\mathbf{\Psi}} := \mathbf{V}^* \mathbf{\Psi}$. While the matrices \mathbf{V} and \mathbf{W} are neither unitary nor independent of $\mathbf{\Omega}$ and $\mathbf{\Psi}$, empirical evidence indicates that the updated test matrices retain sufficient randomness for accurate low-rank approximation throughout the factorization process. Although, in principle, certain directions could be preferentially amplified or suppressed, extensive numerical experiments suggest that this effect is minimal in practice.

4.4. Randomized Strong Recursive Skeletonization. In this section, we describe how the randomized procedure introduced in Section 4.3 can be recursively applied to compute an approximate factorization of \mathbf{A} using only matrix vector products. The sketches drawn of \mathbf{A} can be updated as the algorithm progresses, and structure can be introduced into the test matrices as needed for sketching subblocks of the sparsified matrix as the algorithm progresses. Algorithm 1 provides pseudocode.

As mentioned in Section 3.2, the sketches are updated, instead of being redrawn at every stage of the algorithm. After eliminating the redundant indices for leaf box B_1 , we can update the sketches to instead maintain sketches of the sparsified matrix

$$(52) \quad \tilde{\mathbf{Y}} = \tilde{\mathbf{A}}(\mathbf{A}; B_1) \tilde{\mathbf{\Omega}}, \quad \tilde{\mathbf{Z}} = \tilde{\mathbf{A}}^* \tilde{\mathbf{\Psi}}$$

using formulas (51) to update initially drawn sketches of \mathbf{A} . As mentioned in Remark 2, the diagonalization operators may introduce additive terms in the far-field of adjacent boxes which need to be recompressed at a later step of the algorithm. As such, in order to compute operators \mathbf{V}_2^{-1} , \mathbf{W}_2^{-1} for the next leaf box B_2 , we use block nullification and extraction techniques on the *updated* sketches of $\{\tilde{\mathbf{Y}}, \tilde{\mathbf{\Omega}}, \tilde{\mathbf{Z}}, \tilde{\mathbf{\Psi}}\}$. In order to maintain sketches of diagonalized matrix $\tilde{\mathbf{A}}(\mathbf{A}; B_1, B_2)$, we again apply update formulas (51).

Consider that the points are uniformly distributed and that the leaf level has 2^L boxes. Then, after diagonalizing redundant indices R_1, \dots, R_{2^L} , the accumulated updates of the original matrix \mathbf{A} take the form

$$(53) \quad \tilde{\mathbf{Y}} := \mathbf{V}_{2^L}^{-1} \cdots \mathbf{V}_1^{-1} \mathbf{Y}, \quad \tilde{\mathbf{\Omega}} := \mathbf{W}_{2^L} \cdots \mathbf{W}_1 \mathbf{\Omega},$$

and likewise for the adjoint sketch and test matrices. The test matrix update involves the sparsification operators \mathbf{E}, \mathbf{F} , which are typically well-conditioned, along with the block elimination operators \mathbf{L}, \mathbf{U} . These elimination factors are often well-conditioned as well, since they are unit-triangular with modest off-diagonal entries. As a result, the majority of the ill-conditioning in \mathbf{A} is isolated in the diagonal factor \mathbf{D} of the factorization in (35).

The sparsification operators \mathbf{E}, \mathbf{F} and elimination operators \mathbf{L}, \mathbf{U} are constructed from the sketches of \mathbf{A} , and therefore depend implicitly on the choice of test matrices $\mathbf{\Omega}$ and $\mathbf{\Psi}$. In principle, this dependence introduces a potential risk: the sketching matrices used to approximate \mathbf{A} are also used to define the transformations that update those sketches. However, in practice, this feedback effect appears to be benign. The sparsification and elimination operators are sparse and well-conditioned, and as a result, the updated sketches $(\tilde{\mathbf{Y}}, \tilde{\mathbf{\Omega}})$ remain sufficiently rich to capture the essential subspace information of the sparsified matrix $\hat{\mathbf{A}}$, without needing to redraw independent sketches at each stage of the algorithm.

To generalize the procedure to a multi-level setting, we maintain an active set of indices as defined in (31) and modify the block nullification and extraction formulas accordingly. When skeletonizing a box B , we use the *active* box and neighbor indices, $\mathbf{B}_{\text{active}}$ and $\mathbf{N}_{\text{active}}$, as defined in (32), instead of the original full index sets. In particular, the null space computation used to form the basis matrices in (46) becomes

$$(54) \quad \tilde{\mathbf{Y}}'_{\mathbf{B}_{\text{active}}} = \tilde{\mathbf{Y}}_{\mathbf{B}_{\text{active}}} \text{null} \begin{pmatrix} \tilde{\mathbf{\Omega}}_{\mathbf{B}_{\text{active}}} \\ \tilde{\mathbf{\Omega}}_{\mathbf{N}_{\text{active}}} \end{pmatrix}$$

for modified test matrices $\tilde{\mathbf{Y}}, \tilde{\mathbf{\Omega}}$. At coarser levels of the hierarchy, this computation remains efficient because the number of active near-field indices is relatively small. However, it is important to note that the null space operation implicitly defines a modified test matrix $\tilde{\mathbf{\Omega}}'$ that may include non-zero entries corresponding to *inactive* points as well. A similar observation applies to block extraction. Consequently, the sketches computed at coarser levels accumulate residual errors introduced at finer levels, due to contributions from inactive indices.

One possible approach to mitigating this error accumulation would be to redraw structured test matrices at each level, explicitly controlling for inactive contributions. However, in this work, we deliberately focus on the setting where all samples are drawn once and reused throughout the factorization process. The question of when and how to optimally redraw sketches to control error propagation across levels remains an important direction for future work.

4.5. Algorithm Complexity. In this section, we analyze the sample complexity and computational complexity of Algorithm 1. We assume that the point distribution consists of N total particles organized hierarchically in a d -dimensional tree, with at most m points per leaf box. The total number of boxes is given by

$$(55) \quad n_{\text{boxes}} := n_{\text{leaf}} + n_{\text{tree}}, \quad n_{\text{leaf}} \approx \frac{N}{m}, \quad n_{\text{tree}} \approx \frac{1}{2^d - 1} \cdot \frac{N}{m}.$$

We denote by n_{neigh} the number of neighboring boxes for a given target box (including the box itself), and by n_{child} the number of children per tree box. These are parameters depend on the geometry and remain uniform across boxes in regular grids. For example, in d -dimensional space, $n_{\text{neigh}} = 3^d$ and $n_{\text{child}} = 2^d$ for uniform point distributions.

For clarity, we first analyze the case of uniform point distributions in Section 4.5.1, and then consider the more general case of nonuniform distributions in Section 4.5.2. Throughout, we assume

Algorithm 1 Randomized strong recursive skeletonization

Require: Sketch and test matrices $\{\mathbf{Y}, \mathbf{Z}, \mathbf{\Omega}, \mathbf{\Psi}\}$ of size $N \times s$ satisfying (37).

Ensure: An invertible factorization $\mathbf{A}_{\text{approx}} \approx \mathbf{A}$.

- 1: **for** level $\ell = L$ to 1 **do** ▷ Upward traversal of the tree
 2: **for** each box B at level ℓ **do** ▷ Boxes are ordered $1, 2, \dots$ sequentially, starting from the finest level L and continuing upward.

3: Get relevant active indices:

$$\mathbf{B}_{\text{active}} = \mathbf{B} \cap \text{active}, \quad \mathbf{N}_{\text{active}} = \mathbf{N} \cap \text{active}.$$

4: Compute far-field sketches using block nullification:

$$\mathbf{Y}'_{\mathbf{B}_{\text{active}}} = \mathbf{Y}_{\mathbf{B}_{\text{active}}} \text{null} \begin{pmatrix} \mathbf{\Omega}_{\mathbf{B}_{\text{active}}} \\ \mathbf{\Omega}_{\mathbf{N}_{\text{active}}} \end{pmatrix},$$

$$\mathbf{Z}'_{\mathbf{B}_{\text{active}}} = \mathbf{Z}_{\mathbf{B}_{\text{active}}} \text{null} \begin{pmatrix} \mathbf{\Psi}_{\mathbf{B}_{\text{active}}} \\ \mathbf{\Psi}_{\mathbf{N}_{\text{active}}} \end{pmatrix}.$$

5: Compute the row-ID:

$$[\mathbf{R} \cup \mathbf{S}, \mathbf{T}] = \text{id}(\mathbf{Y}'_{\mathbf{B}_{\text{active}}} + \mathbf{Z}'_{\mathbf{B}_{\text{active}}}).$$

6: Form sparsification operators \mathbf{E}, \mathbf{F} and update sketches:

$$\hat{\mathbf{Y}} \leftarrow \mathbf{E} \mathbf{Y}, \quad \hat{\mathbf{\Omega}} \leftarrow \mathbf{F}^{-1} \mathbf{\Omega},$$

$$\hat{\mathbf{Z}} \leftarrow \mathbf{F}^* \mathbf{Z}, \quad \hat{\mathbf{\Psi}} \leftarrow \mathbf{E}^{-*} \mathbf{\Psi}.$$

7: Extract sparse blocks using block extraction:

$$(\mathbf{X}_{\mathbf{R}\mathbf{B}_{\text{active}}} \quad \mathbf{X}_{\mathbf{R}\mathbf{N}_{\text{active}}}) \approx \mathbf{Y}_{\mathbf{R}} \begin{pmatrix} \mathbf{\Omega}_{\mathbf{B}_{\text{active}}} \\ \mathbf{\Omega}_{\mathbf{N}_{\text{active}}} \end{pmatrix}^{\dagger},$$

$$(\mathbf{X}_{\mathbf{B}_{\text{active}}\mathbf{R}}^* \quad \mathbf{X}_{\mathbf{N}_{\text{active}}\mathbf{R}}^*) \approx \mathbf{Z}_{\mathbf{R}} \begin{pmatrix} \mathbf{\Psi}_{\mathbf{B}_{\text{active}}} \\ \mathbf{\Psi}_{\mathbf{N}_{\text{active}}} \end{pmatrix}^{\dagger}.$$

8: Compute sparse elimination operators \mathbf{L}, \mathbf{U} and update sketches:

$$\tilde{\mathbf{Y}} \leftarrow \mathbf{L} \hat{\mathbf{Y}}, \quad \tilde{\mathbf{\Omega}} \leftarrow \mathbf{U}^{-1} \hat{\mathbf{\Omega}},$$

$$\tilde{\mathbf{Z}} \leftarrow \mathbf{U}^* \hat{\mathbf{Z}}, \quad \tilde{\mathbf{\Psi}} \leftarrow \mathbf{L}^{-*} \hat{\mathbf{\Psi}}.$$

9: Mark \mathbf{R} as inactive.

10: Assign updated sketch and test matrices:

$$\mathbf{Y} \leftarrow \tilde{\mathbf{Y}}, \quad \mathbf{\Omega} \leftarrow \tilde{\mathbf{\Omega}}, \quad \mathbf{Z} \leftarrow \tilde{\mathbf{Z}}, \quad \mathbf{\Psi} \leftarrow \tilde{\mathbf{\Psi}}.$$

11: At the root level, extract the final remaining submatrix:

$$\tilde{\mathbf{A}}_{\mathbf{B}_t \mathbf{B}_t} \approx \tilde{\mathbf{Y}}_{\mathbf{B}_t} \tilde{\mathbf{\Omega}}_{\mathbf{B}_t}^{\dagger}.$$

that far-field interactions can be compressed to a fixed rank k , specified by the user. We denote by p the oversampling parameter used in randomized compression, typically chosen as a small constant (e.g., $p = 10$).

4.5.1. *Uniform Point Distributions.* At the finest level of the tree (i.e., leaf boxes), the dominant costs arise from block nullification and block extraction. For instance, block nullification involves computing the null space of a matrix of size $n_{\text{neigh}} m \times s$. To produce a structured test matrix $\mathbf{\Omega}'$ with $(k + p)$ columns, the number of samples required is

$$s \geq m n_{\text{neigh}} + k + p.$$

The computational complexity of the null-space operation per leaf box is then

$$\mathcal{O}(n_{\text{neigh}}^2 m^2 s) = \mathcal{O}(n_{\text{neigh}}^3 m^3).$$

At coarser levels of the tree (tree boxes), only the active degrees of freedom associated with the box and its neighbors are involved. If each tree box contains $n_{\text{child}} \cdot k$ active points, then the number of samples needed is

$$s \geq (n_{\text{child}} \cdot n_{\text{neigh}} + 1) k + p.$$

For uniform point distributions, the product $n_{\text{child}} \cdot n_{\text{neigh}} = 6^d$ arises frequently in fast multipole methods and \mathcal{H}^2 matrices under strong admissibility conditions, where it is associated with the size of the interaction list.

By choosing the leaf size m such that $m \leq n_{\text{child}} \cdot k$, the sample requirements at the leaf and tree levels become comparable. Consequently, the number of samples needed globally is:

$$(56) \quad s = (6^d + 1) k + p.$$

The total post-processing time to reconstruct the factorization involves processing each of the boxes. Using (55), the total cost is

$$(57) \quad T_{\text{reconstruct}} = \mathcal{O}(n_{\text{neigh}}^3 n_{\text{child}}^2 k^2 N) = \mathcal{O}(108^d k^2 N).$$

This is linear in the problem size, albeit with large problem-dependent constants which depend on the dimensionality as well as the chosen rank parameter. The cost of applying the computed factorization to a vector (i.e., a matrix-vector solve) scales linearly with N as

$$(58) \quad T_{\text{solve}} = \mathcal{O}(6^d k N).$$

This scaling is consistent with the typical costs observed in fast multipole methods and hierarchical matrix factorizations under the strong admissibility condition.

A key advantage of Algorithm 1 is that it requires only a single set of random test matrices, which are reused across all levels via post-processing. This makes it particularly effective for problems where matrix entries are expensive or inaccessible. While the post-processing steps, such as null-space computation and block extraction, introduce a large constant prefactor to the runtime, this overhead is often offset by the substantial savings in sample complexity.

4.5.2. Nonuniform Point Distributions. For nonuniform point distributions, the number of active degrees of freedom per box can vary significantly depending on the local point density and the geometry of the domain. As a result, the sample complexity is no longer uniform across all boxes, and must instead adapt to the local number of active points.

Specifically, the number of samples required for a given box B is determined by the sum of the degrees of freedom active degrees of freedom, consisting of neighboring boxes at both the leaf and tree levels. In particular, the number of samples needed for box B is given by:

$$s_B = (k + p) + \sum_{\substack{\text{tree box } B' \\ \text{neighboring } B}} \min(k, |B'|) + \sum_{\substack{\text{leaf box } B' \\ \text{neighboring } B}} |B'|$$

where $|B'|$ denotes the number of points in box B' . The quantity $\min(k, |B'|)$ reflects the fact that tree boxes may have fewer than k active points, especially near boundaries or in highly nonuniform distributions. The overall sample complexity is therefore determined by the worst-case number of samples across all boxes:

$$s = \max_B s_B.$$

The computational complexity of post-processing samples is

$$T_{\text{reconstruct}} = \mathcal{O}\left(s^3 \frac{N}{m}\right),$$

where m is set to be some reasonable quantity depending on the geometry as well the rank parameter. Compared to the uniform setting, nonuniform point distributions introduce variability in both the number of samples required and the per-box computational cost. Nevertheless, Algorithm 1 retains its key advantage: a single set of random samples is drawn and reused throughout the factorization, independent of the underlying point distribution. In many practical settings — particularly when points lie on a lower-dimensional manifold (e.g., a surface in 3D) — the number of samples required is often substantially smaller than that needed for a uniform distribution in d -dimensions.

5. NUMERICAL RESULTS

In this section, we illustrate the performance of the proposed algorithm. The user specifies a parameter k that controls the target rank used for low-rank approximation. The RSRS algorithm operates on a hierarchical tree \mathcal{T} , where the leaves are partitioned to contain at most ck points, with $c = \{4, 6\}$ for two- and three-dimensional geometries, respectively.

We assess the accuracy of the computed factorization $\mathbf{A}_{\text{approx}} \approx \mathbf{A}$ both in terms of the factorization error and the quality of the approximate inverse. Specifically, we report:

$$(59) \quad \text{relerr} = \frac{\|\mathbf{A} - \mathbf{A}_{\text{approx}}\|_2}{\|\mathbf{A}\|_2}, \quad \text{errsolve} = \|\mathbf{I} - \mathbf{A}_{\text{approx}}^{-1} \mathbf{A}\|_2$$

which are two quantities estimated using a power iteration. When using $\mathbf{A}_{\text{approx}}^{-1}$ as a direct solver or as a preconditioner for \mathbf{A} , the effectiveness of the approximation depends on the condition number of \mathbf{A} . In particular, if $\text{relerr} \leq \epsilon$, then for a solution $\mathbf{x} = \mathbf{A}^{-1} \mathbf{b}$ and its approximation $\tilde{\mathbf{x}} = \mathbf{A}_{\text{approx}}^{-1} \mathbf{b}$, the relative error is bounded by

$$(60) \quad \frac{\|\mathbf{x} - \tilde{\mathbf{x}}\|}{\|\mathbf{x}\|} \leq \frac{2 \epsilon \text{cond}(\mathbf{A})}{1 - \epsilon \text{cond}(\mathbf{A})}.$$

Thus, higher condition numbers may require larger rank parameter k to maintain solver accuracy. In the numerical experiments, we consider a variety of PDE discretizations and study the performance of the factorization as the matrix size N increases. In many cases, such as Section 5.1, the condition number $\text{cond}(\mathbf{A})$ grows with N , increasing the difficulty of achieving high-accuracy solves.

Additional challenges arise for indefinite problems, such as the Helmholtz equation, where the underlying system is more challenging to precondition or solve. Nevertheless, the numerical results demonstrate that RSRS is robust to both ill-conditioning and indefiniteness. In addition to reporting the metrics in Table 1, we also measure the number of GMRES iterations required to solve \mathbf{A} directly, and the number of iterations when using $\mathbf{A}_{\text{approx}}^{-1}$ as a preconditioner. The experiments were performed on a machine equipped with an Intel Xeon Gold 6254 CPU and 768GB of RAM. Although the system features a multi-core architecture, the current implementation employs limited parallelism; each operation on every box is executed sequentially.

N	number of points
k	rank parameter
N_{samples}	number of matrix-vector samples of \mathbf{A} and \mathbf{A}^*
$T_{\text{reconstruct}}$	wall-clock time to construct $\mathbf{A}_{\text{approx}}^{-1}$ (in seconds)
relerr	defined in equation (59)
errsolve	
niter	number of GMRES iterations required to reach relative tolerance $\text{rtol}=10^{-10}$

TABLE 1. Summary of notation used in reported numerical results.

5.1. Example 1: Integral Equation on a 2D Grid. Consider a volume integral for the Laplace equation discretized on a unit square $\Omega = [0, 1]^2$. The collocation points \mathbf{x} are placed on a uniform grid of $\sqrt{N} \times \sqrt{N}$ points, and matrix entries are given by

$$\mathbf{A}_{ij} = \frac{1}{N} \log(\|\mathbf{x}_i - \mathbf{x}_j\|), \quad i \neq j$$

$$\mathbf{A}_{ii} \approx \int_{-h/2}^{h/2} \int_{-h/2}^{h/2} \log(\|\mathbf{x}_i - \mathbf{x}_j\|) d\mathbf{x}_i d\mathbf{x}_j, \quad \text{where } h \equiv 1/\sqrt{N},$$

and where modified entries on the diagonal are approximated using the Quadpack library [41]. Because the collocation points are on a uniform grid, the matrix \mathbf{A} and its adjoint can be applied to vectors in $\mathcal{O}(N \log N)$ time using the FFT [17]. This example appeared previously in [40].

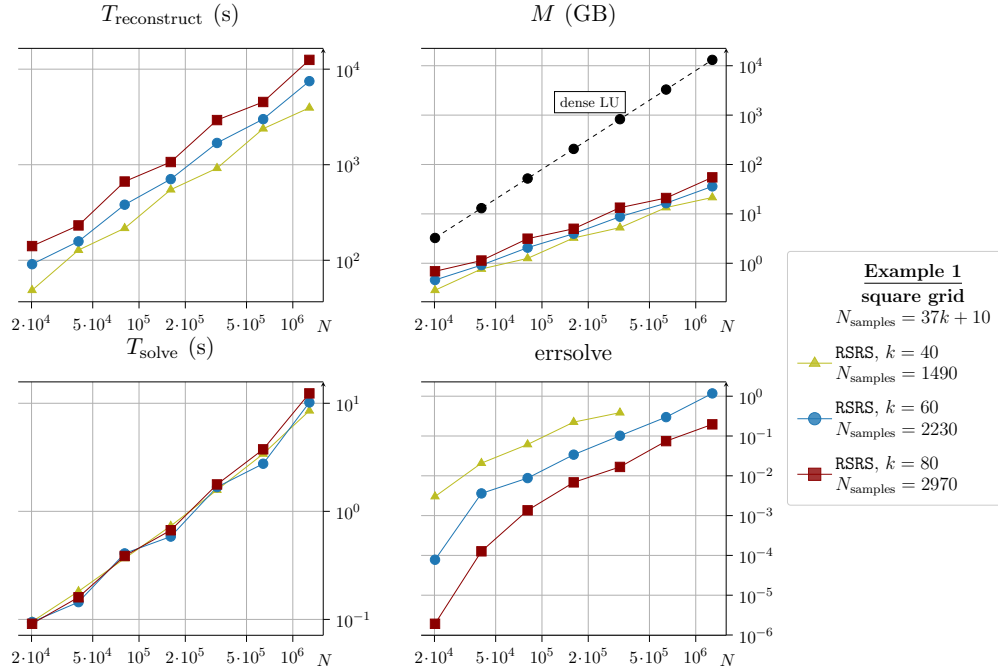


FIGURE 5. Performance of RSRS for Example 1.

N	$\text{cond}(\mathbf{A})$	RSRS, $k = 60$ $N_{\text{samples}} = 2230$		RSRS, $k = 80$ $N_{\text{samples}} = 2970$	
		relerr	errsolve	relerr	errsolve
20,000	2.8e+04	3.0e-08	7.8e-05	1.6e-06	1.9e-06
80,000	1.2e+05	1.2e-06	8.8e-03	4.4e-07	1.4e-03
321,000	5.1e+05	8.9e-06	1.0e-01	1.9e-06	1.7e-02
1,281,000	2.1e+06	2.2e-04	1.2e+00	2.4e-05	2.0e-01

(A) Accuracy and solver effectiveness.

N	No preconditioner	RSRS, $k = 60$	RSRS, $k = 80$
	niter	niter	niter
20,000	1,420	3	3
80,000	4,910	5	4
321,000	>10,000	9	6
1,281,000	>10,000	53	12

(B) Preconditioner performance.

TABLE 2. Summary of results for Example 1. Left: Accuracy of the computed factorization and its effectiveness as a solver for increasing problem size N . Right: Preconditioner performance across a range of problem sizes, showing that despite worsening conditioning, the factorization remains effective.

The matrix is the discretization of a first-kind integral equation, and the matrix suffers from the effects of ill-conditioning, with worsening condition number as N increases. Despite the effects of ill-conditioning, RSRS is effective as preconditioner with a modest number of samples needed to construct the factorization. Figure 5 summarizes relevant measured quantities as well as the sample costs for each rank parameter k . Table 2 reports the effectiveness as a solver as well as a preconditioner. The number of samples is exactly $N_{\text{samples}} = (6^2 + 1)k + 10$, as analyzed in Section 4.5, as expected for a uniform geometry.

5.2. Example 2: Second-Kind Boundary Integral Equation on Sphere Surface. We consider the Dirichlet problem for the Laplace equation inside the unit sphere, which we denote Ω . Given Dirichlet data f defined on the surface of the unit sphere $\partial\Omega$, we aim to find the solution u which satisfies

$$(61) \quad \Delta u(x) = 0 \quad \text{for } x \in \Omega, \quad u(x) = f(x) \quad \text{for } x \in \partial\Omega.$$

To solve (61), we represent the solution using a double-layer potential, for some function $\sigma(x)$ defined on the boundary

$$(62) \quad u(x) = \int_{\partial\Omega} \frac{\partial G}{\partial n_y}(x - y) \sigma(y) dy,$$

where $G(x) = \frac{1}{4\pi\|x\|}$ is the free-space Green's function for the Laplace equation in \mathbb{R}^3 , $\frac{\partial G}{\partial n_y}$ denotes the normal derivative with respect to the source variable y , and n_y is the outward-pointing normal at point $y \in \partial\Omega$. Imposing the Dirichlet condition yields a second-kind Fredholm integral equation to be solved for the unknown $\sigma(x)$

$$(63) \quad -\frac{1}{2}\sigma(x) + \int_{\partial\Omega} \frac{\partial G}{\partial n_y}(x - y) \sigma(y) dy = f(x), \quad x \in \partial\Omega.$$

To discretize (63), we represent $\partial\Omega$ as a mesh of flat triangular panels. The centroids of these triangles are used as collocation points in the numerical method. To accurately evaluate integrals involving near-field interactions, we employ fourth-order tensor-product Gauss–Legendre quadrature. The resulting linear system is nonsymmetric due to both the nature of the integral kernel and the geometry of the discretized surface. The discretized system is applied rapidly to vectors using the FMM [5]. This example previously appeared in [40].

The boundary integral equation (63) has the form of $\mathbf{I} + \mathbf{G}$, where the latter term \mathbf{G} is a compact operator. Because it is a compact perturbation of the identity operator, the resulting discretized system is well conditioned, and as reported in Table 3, the condition number of the system is constant as the number of discretization points N increases. As a result, GMRES converges in only a few iterations, and a preconditioner is not necessary. We include this example as a numerical benchmark to demonstrate the performance of the algorithm without the effects of ill-conditioning.

		RSRS, $k = 20$		RSRS, $k = 40$		RSRS, $k = 60$	
		$N_{\text{samples}} = 1673$		$N_{\text{samples}} = 3028$		$N_{\text{samples}} = 4468$	
N	cond(\mathbf{A})	relerr	errsolve	relerr	errsolve	relerr	errsolve
20,000	2.0e+00	3.9e-05	8.4e-05	1.6e-06	6.8e-06	2.3e-07	4.6e-07
81,000	2.0e+00	1.6e-04	3.2e-04	5.8e-06	1.1e-05	1.9e-06	8.5e-07
327,000	2.0e+00	3.2e-04	6.1e-04	3.3e-05	6.0e-05	3.9e-06	9.6e-06
1,310,000	2.0e+00	9.6e-04	1.8e-03	7.7e-05	1.5e-04	1.5e-05	2.9e-05

TABLE 3. A summary of the computed accuracy and effectiveness as a solver for increasing problem size N for Example 2.

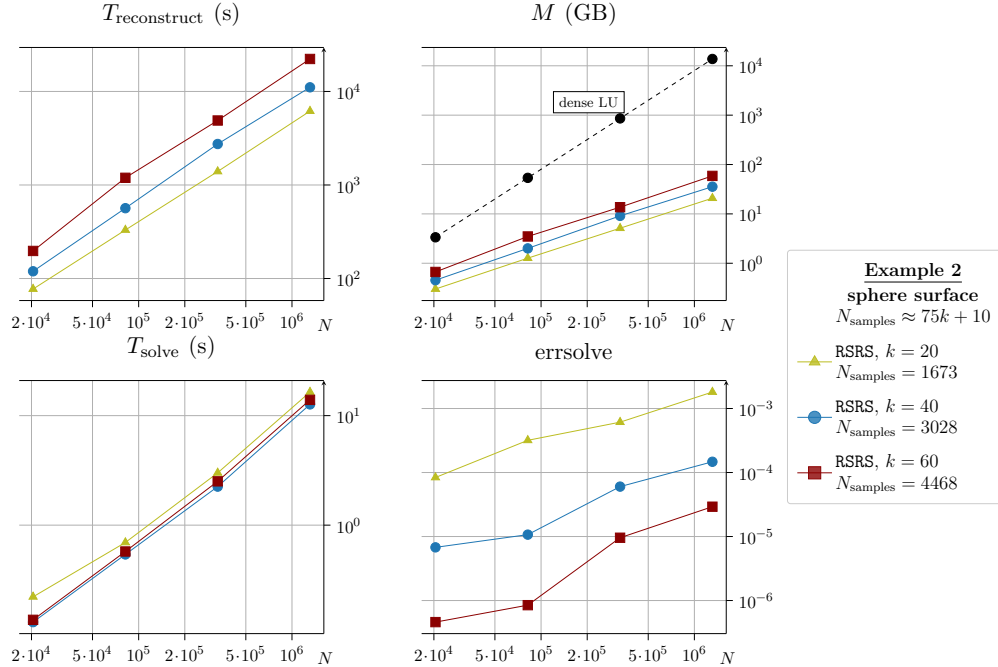


FIGURE 6. Performance of RSRs for Example 2.

Figure 6 summarizes the key performance metrics and sample costs for different rank parameters k , while Table 3 reports the effectiveness of the factorization both as a compression scheme and as a solver. The total number of samples used is $N_{\text{samples}} \approx 95k + 10$, which reflects the maximum number of samples required across all boxes to perform block nullification and extraction. Since \mathbf{A} is well-conditioned, the observed values of relerr and errsolve are nearly identical. However, we note a slight degradation in accuracy as the problem size increases from $N = 20,000$ to $N = 1.3$ million, despite using a fixed number of samples. This loss in accuracy may result from the accumulation of numerical errors across multiple levels of the randomized algorithm. Selectively resketching at certain levels could potentially mitigate this effect, though it would incur additional sampling costs.

5.3. Example 3: Schur Complement Preconditioner for Sparse Solvers. In this example, we demonstrate how \mathcal{H}^2 matrix factorizations can be leveraged to improve the complexity and memory footprint of sparse solvers, building upon prior work [45, 46, 49]. We consider the 3D Helmholtz equation,

$$(64) \quad (-\Delta - \kappa^2)u(x) = f(x), \quad x \in [0, 1]^3.$$

discretized using a standard 7-point finite difference stencil on a uniform grid. The resulting sparse matrix \mathbf{A} has the familiar 7-point stencil sparsity pattern, illustrated in Figure 7. We set the wavenumber as $\kappa := 13.6$ so that there are about two wavelengths across the unit domain.

To factorize \mathbf{A} , we partition the domain into eight interior gray octants and a top-level separator I_1 , as shown in Figure 7. The interior octants are eliminated recursively first, and the separator I_1 is eliminated last. This ordering minimizes fill-in and isolates dense Schur complements to smaller

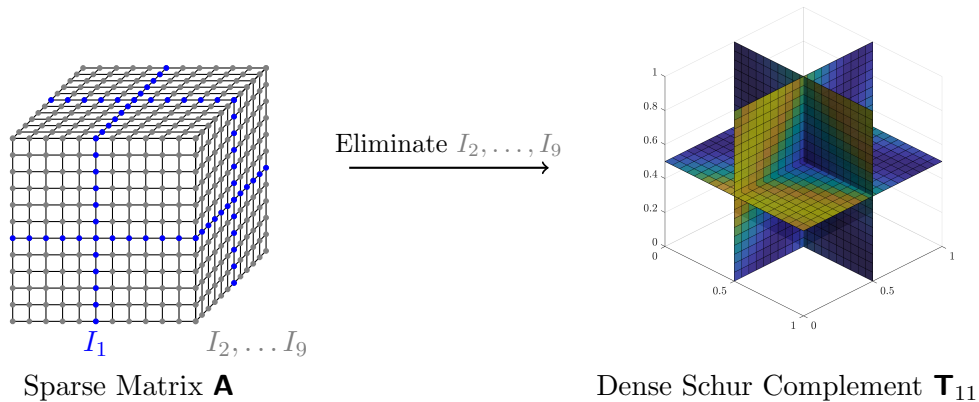


FIGURE 7. Discretization of the 3D Helmholtz equation using a 7-point stencil produces a sparse matrix \mathbf{A} (left). Eliminating the gray interior octants results in a dense Schur complement on the separator I_1 (right).

separators. The sparsity pattern of \mathbf{A} after this reordering is:

$$(65) \quad \mathbf{A} = \begin{bmatrix} \mathbf{A}_{99} & & & & \mathbf{A}_{91} \\ & \mathbf{A}_{88} & & & \mathbf{A}_{81} \\ & & \ddots & & \vdots \\ & & & \mathbf{A}_{22} & \mathbf{A}_{21} \\ \mathbf{A}_{19} & \mathbf{A}_{18} & \dots & \mathbf{A}_{12} & \mathbf{A}_{11} \end{bmatrix},$$

with an associated invertible factorization $\mathbf{A} = \mathbf{L} \mathbf{D} \mathbf{U}$, where \mathbf{L} and \mathbf{U} are sparse triangular factors, and \mathbf{D} is block diagonal with the Schur complement \mathbf{T}_{11} on I_1 , defined by:

$$(66) \quad \mathbf{T}_{11} = \mathbf{A}_{11} - \sum_{j=2}^9 \mathbf{A}_{1j} \mathbf{A}_{jj}^{-1} \mathbf{A}_{j1}.$$

Each factor $\mathbf{A}_{jj}^{-1} \mathbf{A}_{j1}$ is dense, leading to a dense Schur complement \mathbf{T}_{11} . The matrices \mathbf{A}_{jj} correspond to sparse subdomains that can be efficiently factorized using standard sparse direct solvers. Applying \mathbf{A}_{jj}^{-1} to a vector requires $\mathcal{O}(N^{4/3})$ operations, making the application of \mathbf{T}_{11} and its adjoint efficient when amortized over multiple right-hand sides. Figure 8 summarizes the numerical results for this experiment, while Table 4 reports the iteration counts for solving the Schur complement system using GMRES, both with and without the **RSRS**-based preconditioner.

6. CONCLUSIONS

This manuscript introduces **RSRS**, an algorithm for simultaneously compressing and inverting \mathcal{H}^2 matrices in matrix-free settings. By leveraging novel randomized sketching techniques, **RSRS** constructs an approximate invertible factorization using random sketches of the matrix and its adjoint. Dense Gaussian test matrices are used for sketching, and the necessary structure is introduced via linear algebraic post-processing techniques, eliminating the need for carefully structured test matrices and avoiding excessive sample costs.

The algorithm builds on and extends recently proposed LU factorization methods for \mathcal{H}^2 matrices [40, 42], adapting them to settings where matrix entries are inaccessible. Its effectiveness is demonstrated across a range of applications, including both integral and differential equations. For ill-conditioned problems where iterative solvers fail to converge, **RSRS** computes a highly effective preconditioner using only a modest number of matrix and adjoint-vector products. Additionally,

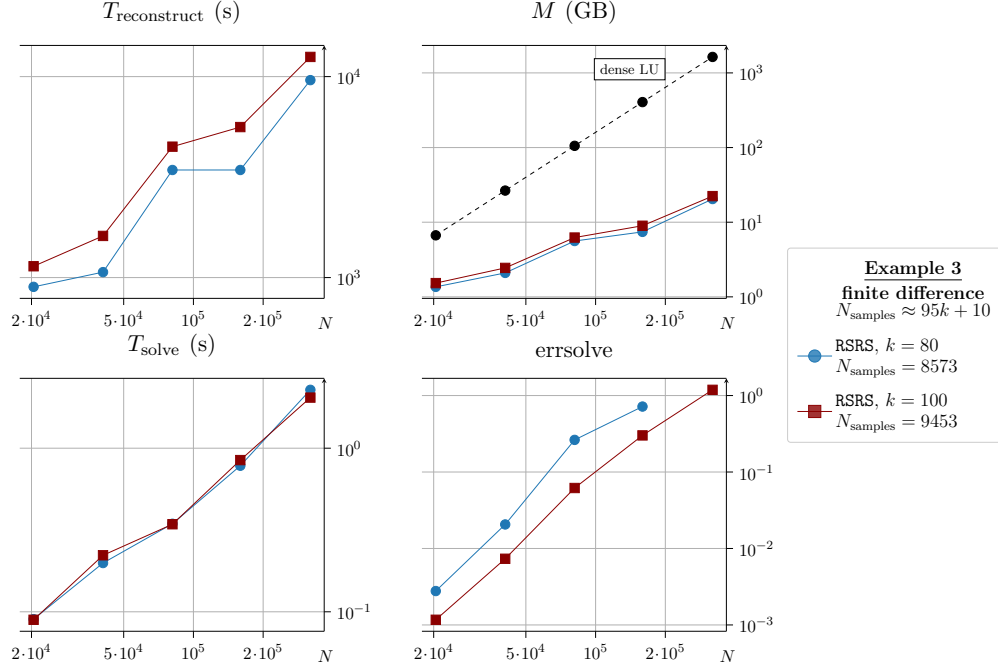


FIGURE 8. Performance of RSRS for Example 3.

N	No preconditioner		RSRS, $k = 80$	RSRS, $k = 100$
	$\text{cond}(\mathbf{T}_{11})$	niter	$N_{\text{samples}} = 8491$	$N_{\text{samples}} = 9371$
			niter	niter
20,000	1.9e+03	>10,000	5	4
40,000	2.6e+03	>10,000	7	5
81,000	3.6e+03	>10,000	10	7
159,000	5.1e+03	>10,000	14	11
319,000	7.2e+03	>10,000	20	15

TABLE 4. Iteration counts for GMRES applied to Example 3. The Helmholtz equation leads to an ill-conditioned Schur complement whose condition number grows with the mesh size. While RSRS does not achieve high-accuracy solves as a standalone method in this setting, it is highly effective as a preconditioner, significantly reducing GMRES iterations.

the algorithm achieves substantial efficiency gains in problems with multiple right-hand sides, with sampling costs amortized even for a single solve.

RSRS opens several promising avenues for future research. These include the analysis of sketch accuracy under recursive transformations, high-performance implementations in distributed environments, and hybrid strategies that combine weak and strong admissibility to balance computational cost and accuracy. Beyond PDEs and integral equations, the method has potential applications in inverse problems, uncertainty quantification, and PDE-constrained optimization—particularly in settings where the matrix is only accessible via its action, and robust fast solvers are essential for tackling large, complex problems.

Acknowledgments. The work reported was supported by the Office of Naval Research (N00014-18-1-2354), by the National Science Foundation (DMS-1952735 and DMS-2313434), and by the Department of Energy ASCR (DE-SC0022251).

Data Availability. Not applicable.

DECLARATIONS

Conflict of Interest. The authors have no relevant financial or non-financial interests to disclose.

REFERENCES

- [1] Nicholas Vieau Alger. *Data-scalable Hessian preconditioning for distributed parameter PDE-constrained inverse problems*. The University of Texas at Austin, 2019.
- [2] Ilona Ambartsumyan, Wajih Boukaram, Tan Bui-Thanh, Omar Ghattas, David Keyes, Georg Stadler, George Turkiyyah, and Stefano Zampini. Hierarchical matrix approximations of Hessians arising in inverse problems governed by PDEs. *SIAM Journal on Scientific Computing*, 42(5):A3397–A3426, 2020.
- [3] Sivaram Ambikasaran and Eric Darve. The inverse fast multipole method. *arXiv preprint arXiv:1407.1572*, 2014.
- [4] Patrick Amestoy, Alfredo Buttari, Jean-Yves l’Excellent, and Theo Mary. On the complexity of the block low-rank multifrontal factorization. *SIAM Journal on Scientific Computing*, 39(4):A1710–A1740, 2017.
- [5] T. Askham, L. Greengard, L. Lu, J. Magland, D. Malhotra, M. O’Neil, and M. Rachh. Flatiron institute fast multipole libraries for the Laplace and Helmholtz kernels in three dimensions., 2021.
- [6] R Beatson and Leslie Greengard. *A short course on fast multipole methods*, pages 1–37. Numerical Mathematics and Scientific Computation. Oxford University Press, 1997.
- [7] Mario Bebendorf. Approximation of boundary element matrices. *Numerische Mathematik*, 86:565–589, 2000.
- [8] Mario Bebendorf. *Hierarchical matrices*, volume 63 of *Lecture Notes in Computational Science and Engineering*. Springer-Verlag, Berlin, 2008. A means to efficiently solve elliptic boundary value problems.
- [9] Mario Bebendorf and Sergej Rjasanow. Adaptive low-rank approximation of collocation matrices. *Computing*, 70:1–24, 2003.
- [10] Steffen Börm. *Efficient numerical methods for non-local operators*, volume 14 of *EMS Tracts in Mathematics*. European Mathematical Society (EMS), Zürich, 2010. \mathcal{H}^2 -matrix compression, algorithms and analysis.
- [11] Steffen Börm and Lars Grasedyck. Hybrid cross approximation of integral operators. *Numerische Mathematik*, 101(2):221–249, Aug 2005.
- [12] Steffen Börm, Lars Grasedyck, and Wolfgang Hackbusch. Introduction to hierarchical matrices with applications. *Engineering analysis with boundary elements*, 27(5):405–422, 2003.
- [13] Nicolas Boullé, Christopher J Earls, and Alex Townsend. Data-driven discovery of Green’s functions with human-understandable deep learning. *Scientific reports*, 12(1):4824, 2022.
- [14] Nicolas Boullé and Alex Townsend. A mathematical guide to operator learning. *arXiv preprint arXiv:2312.14688*, 2023.
- [15] Chao Chen and Per-Gunnar Martinsson. Solving linear systems on a GPU with hierarchically off-diagonal low-rank approximations. In *Proceedings of the International Conference on High Performance Computing, Networking, Storage and Analysis*, SC ’22. IEEE Press, 2022.
- [16] H. Cheng, Z. Gimbutas, P.G. Martinsson, and V. Rokhlin. On the compression of low rank matrices. *SIAM Journal of Scientific Computing*, 26(4):1389–1404, 2005.
- [17] James W Cooley and John W Tukey. An algorithm for the machine calculation of complex Fourier series. *Mathematics of computation*, 19(90):297–301, 1965.
- [18] Yijun Dong and Per-Gunnar Martinsson. Simpler is better: a comparative study of randomized pivoting algorithms for CUR and interpolative decompositions. *Advances in Computational Mathematics*, 49, 08 2023.
- [19] Adrianna Gillman, Patrick Young, and Per-Gunnar Martinsson. A direct solver $\mathcal{O}(n)$ complexity for integral equations on one-dimensional domains. *Frontiers of Mathematics in China*, 7:217–247, 2012. 10.1007/s11464-012-0188-3.
- [20] Lars Grasedyck. Adaptive recompression of matrices for BEM. *Computing*, 74:205–223, 2005.
- [21] L. Greengard and V. Rokhlin. A fast algorithm for particle simulations. *J. Comput. Phys.*, 73(2):325–348, 1987.
- [22] Leslie Greengard and Vladimir Rokhlin. A new version of the fast multipole method for the Laplace equation in three dimensions. In *Acta numerica, 1997*, volume 6 of *Acta Numer.*, pages 229–269. Cambridge Univ. Press, Cambridge, 1997.
- [23] Ming Gu and Stanley C. Eisenstat. Efficient algorithms for computing a strong rank-revealing QR factorization. *SIAM J. Sci. Comput.*, 17(4):848–869, 1996.
- [24] Wolfgang Hackbusch et al. *Hierarchical matrices: algorithms and analysis*, volume 49. Springer, 2015.

- [25] Nathan Halko, Per-Gunnar Martinsson, and Joel A. Tropp. Finding structure with randomness: Probabilistic algorithms for constructing approximate matrix decompositions. *SIAM Review*, 53(2):217–288, 2011.
- [26] Kenneth L. Ho and Leslie Greengard. A fast direct solver for structured linear systems by recursive skeletonization. *SIAM Journal on Scientific Computing*, 34(5):A2507–A2532, 2012.
- [27] Tobin Isaac, Noemi Petra, Georg Stadler, and Omar Ghattas. Scalable and efficient algorithms for the propagation of uncertainty from data through inference to prediction for large-scale problems, with application to flow of the antarctic ice sheet. *Journal of Computational Physics*, 296:348–368, 2015.
- [28] James Levitt. *Building rank-revealing factorizations with randomization*. PhD thesis, University of Texas at Austin, 2022.
- [29] James Levitt and Per-Gunnar Martinsson. Linear-complexity black-box randomized compression of rank-structured matrices. *SIAM Journal on Scientific Computing*, 46(3):A1747–A1763, 2024.
- [30] Edo Liberty, Franco Woolfe, Per-Gunnar Martinsson, Vladimir Rokhlin, and Mark Tygert. Randomized algorithms for the low-rank approximation of matrices. *Proc. Natl. Acad. Sci. USA*, 104(51):20167–20172, 2007.
- [31] L. Lin, J. Lu, and L. Ying. Fast construction of hierarchical matrix representation from matrix-vector multiplication. *Journal of Computational Physics*, 230(10):4071 – 4087, 2011.
- [32] Per-Gunnar Martinsson. A fast direct solver for a class of elliptic partial differential equations. *J. Sci. Comput.*, 38(3):316–330, 2009.
- [33] Per-Gunnar Martinsson. Compressing rank-structured matrices via randomized sampling. *SIAM Journal on Scientific Computing*, 38(4):A1959–A1986, 2016.
- [34] Per-Gunnar Martinsson. *Fast Direct Solvers for Elliptic PDEs*, volume CB96 of *CBMS-NSF conference series*. SIAM, 2019.
- [35] Per-Gunnar Martinsson, Vladimir Rokhlin, Yoel Shkolnisky, and Mark Tygert. Id: A software package for low-rank approximation of matrices via interpolative decompositions, version 0.2, 2008.
- [36] Per-Gunnar Martinsson, Vladimir Rokhlin, and Mark Tygert. A randomized algorithm for the decomposition of matrices. *Appl. Comput. Harmon. Anal.*, 30(1):47–68, 2011.
- [37] Per-Gunnar Martinsson and Joel A. Tropp. Randomized numerical linear algebra: Foundations and algorithms. *Acta Numerica*, 29:403–572, 2020.
- [38] P.G. Martinsson. A fast randomized algorithm for computing a hierarchically semiseparable representation of a matrix. *SIAM Journal on Matrix Analysis and Applications*, 32(4):1251–1274, 2011.
- [39] P.G. Martinsson and V. Rokhlin. A fast direct solver for boundary integral equations in two dimensions. *J. Comp. Phys.*, 205(1):1–23, 2005.
- [40] Victor Minden, Kenneth L. Ho, Anil Damle, and Lexing Ying. A recursive skeletonization factorization based on strong admissibility. *Multiscale Modeling & Simulation*, 15(2):768–796, 2017.
- [41] Robert Piessens, Elise de Doncker-Kapenga, Christoph W Überhuber, and David K Kahaner. *Quadpack: a subroutine package for automatic integration*, volume 1. Springer Science & Business Media, 2012.
- [42] Daria Sushnikova, Leslie Greengard, Michael O’Neil, and Manas Rachh. FMM-LU: A fast direct solver for multiscale boundary integral equations in three dimensions. *Multiscale Modeling & Simulation*, 21(4):1570–1601, 2023.
- [43] S. Voronin and P.-G. Martinsson. Efficient algorithms for CUR and interpolative matrix decompositions. *Advances in Computational Mathematics*, 43(3):495–516, 2017.
- [44] J. Xia, S. Chandrasekaran, M. Gu, and X.S. Li. Fast algorithms for hierarchically semiseparable matrices. *Numerical Linear Algebra with Applications*, 17(6):953–976, 2010.
- [45] Jianlin Xia. Randomized sparse direct solvers. *SIAM Journal on Matrix Analysis and Applications*, 34(1):197–227, 2013.
- [46] Jianlin Xia, Shivkumar Chandrasekaran, Ming Gu, and Xiaoye S. Li. Superfast multifrontal method for large structured linear systems of equations. *SIAM J. Matrix Anal. Appl.*, 31(3):1382–1411, 2010.
- [47] Xin Xing and Edmond Chow. Interpolative decomposition via proxy points for kernel matrices. *SIAM Journal on Matrix Analysis and Applications*, 41(1):221–243, 2020.
- [48] Xin Ye, Jianlin Xia, and Lexing Ying. Analytical low-rank compression via proxy point selection. *SIAM Journal on Matrix Analysis and Applications*, 41(3):1059–1085, 2020.
- [49] Anna Yesypenko and Per-Gunnar Martinsson. SlabLU: a two-level sparse direct solver for elliptic pdes. *Advances in Computational Mathematics*, 50(4):90, 2024.